Fermi Surface, Pseudopotential Coefficients, and Spin-Orbit Coupling in Lead*

J. R. ANDERSON† AND A. V. GOLD‡
Institute for Atomic Research and Department of Physics, Iowa State University, Ames, Iowa
(Received 18 March 1965)

The de Haas–van Alphen periods in lead have been studied in 200 kG impulsive fields, employing techniques with sensitivity and selectivity which are far improved over those used in an earlier study of this metal, and several new sets of oscillations have been discovered. The results confirm in detail the correctness of a nearly-free-electron Fermi surface based on four conduction electrons per atom, and the experimentally determined Fermi surface has been described in terms of an interpolation scheme using four orthogonalized plane waves for each wave vector **k**. As would be expected for a heavy metal such as lead, it is necessary to allow for the large spin-orbit interaction in order to achieve an accurate description of all portions of the Fermi surface. The four adjustable parameters required in the description have been determined by a least-squares fit to eight observed extremal areas of cross section, and are found to be (in Ry): Fermi energy $E_f=0.718\pm0.001$; Fourier coefficients of the pseudopotential $V_{111}=-0.084\pm0.002$ and $V_{200}=-0.039\pm0.002$; and spin-orbit interaction $\lambda=0.096\pm0.002$. These values of the parameters refer to a specific interpolation scheme and assume that the mass in the kinetic-energy matrix elements is the free-electron mass (i.e., no attempt has been made to consider explicitly many-body effects or the electron-phonon interaction). When the above parameters are used, the total occupied volume is calculated to correspond to 4.02 ± 0.02 electrons per atom, and the model confirms the experimental finding that the fourth zone is empty. The calculated dispersion curves $E(\mathbf{k})$ reflect the 'inert-pair' behavior which is so well known in the chemistry of lead salts, in that there is a large energy gap between a filled 6*s*-like band and the lowest branch of the 6*p*-like bands which is never less than 0.13 Ry. The predictions of the model as regards the detailed orientation dependence of the de Haas–van Alphen periods are found to be in excellent agreement with experiment; comparison is also made with the Fermi-surface dimensions, cyclotron masses, magnetoresistance, etc., as determined by other experiments.

INTRODUCTION

ON the basis of an earlier study of the de Haas–van Alphen effect in lead using 80 kG impulsive fields,[1] a simple, nearly-free-electron model was advanced as a plausible approximation to the actual Fermi surface. At that time the limitations of the experimental technique were such that only a few oscillatory terms were observed in the susceptibility; however, if the simple model for the Fermi surface were to have any real validity, further oscillatory terms would be expected. In this research we have succeeded in finding several of the predicted oscillations by extending the range of fields to 200 kG, by improving otherwise the sensitivity of the impulsive-field technique, and by using single crystals of much greater perfection than those used earlier.

In the meantime, several authors have reported measurements of various properties of lead which are also directly related to the Fermi surface. These results are from the magnetoresistance effect,[2–4] ultrasonic attenuation,[5,6] cyclotron resonance[7,3,8] and the Kohn effect,[9–11] and they have all been interpreted, with varying degrees of accuracy and reliability, in terms of features which are predicted by the nearly-free-electron model. The new de Haas–van Alphen measurements presented in this paper also confirm the basic correctness of the simple model; moreover, the present results are of sufficient detail and accuracy to permit a really quantitative description of the Fermi surface to be attempted.

The use of pseudopotential theory in accounting for the band structures and the Fermi surfaces of nontransition metals is now well established,[12–18] and we have used an interpolation scheme with four orthogonalized plane waves (OPW's) for each wave vector **k** to describe the lead Fermi surface. In this model, the

* Contribution No. 1648. The major part of this research was carried out in the Ames Laboratory of the U. S. Atomic Energy Commission.
† National Science Foundation Graduate Fellow 1960–1962; National Science Foundation Postdoctoral Fellow, Royal Society Mond Laboratory, University of Cambridge 1963. Present address: Department of Physics and Astronomy, University of Maryland, College Park, Maryland.
‡ Alfred P. Sloan Research Fellow.
[1] A. V. Gold, Phil. Trans. Roy. Soc. (London) **A251**, 85 (1958).
[2] N. E. Alekseyevsky and Yu. P. Gaidukov, Zh. Eksperim. i Teor. Fiz. **41**, 354 (1961) [English transl.: Soviet Phys.—JETP **14**, 256 (1962)].
[3] R. C. Young, Phil. Mag. **7**, 2065 (1962). The interpretation of magnetoresistance data (Ref. 2) is discussed in the appendix to Young's paper.
[4] J. E. Schirber, Phys. Rev. **131**, 2459 (1963).
[5] A. R. Mackintosh, Proc. Roy. Soc. (London) **A271**, 88 (1963).
[6] J. A. Rayne, Phys. Rev. **129**, 652 (1963).
[7] M. S. Khaikin and R. T. Mina, Zh. Eksperim. i Teor. Fiz. **42**, 35 (1962) [English transl.: Soviet Phys.—JETP **15**, 24 (1962)].
[8] R. T. Mina and M. S. Khaikin, Zh. Eksperim. i Teor. Fiz. **45**, 1304 (1963) [English transl.: Soviet Phys.—JETP **18**, 896 (1964)].
[9] B. N. Brockhouse, K. R. Rao, and A. D. B. Woods, Phys. Rev. Letters **7**, 93 (1961).
[10] B. N. Brockhouse, T. Arase, G. Caglioti, K. R. Rao, and A. D. B. Woods, Phys. Rev. **128**, 1099 (1962).
[11] A. Paskin and R. J. Weiss, Phys. Rev. Letters **9**, 199 (1962).
[12] J. C. Phillips and L. Kleinman, Phys. Rev. **116**, 287 (1959).
[13] W. A. Harrison, Phys. Rev. **118**, 1182 (1960).
[14] W. A. Harrison, Phys. Rev. **118**, 1190 (1960).
[15] M. H. Cohen and V. Heine, Phys. Rev. **122**, 1821 (1961).
[16] W. A. Harrison, Phys. Rev. **126**, 497 (1962).
[17] J. R. Anderson, Ph.D. dissertation, Iowa State University (1962); available as U. S. Atomic Energy Commission Report IS–762 from Office of Technical Services, Department of Commerce, Washington 25, D. C.
[18] N. W. Ashcroft, Phil. Mag. **8**, 2055 (1963).

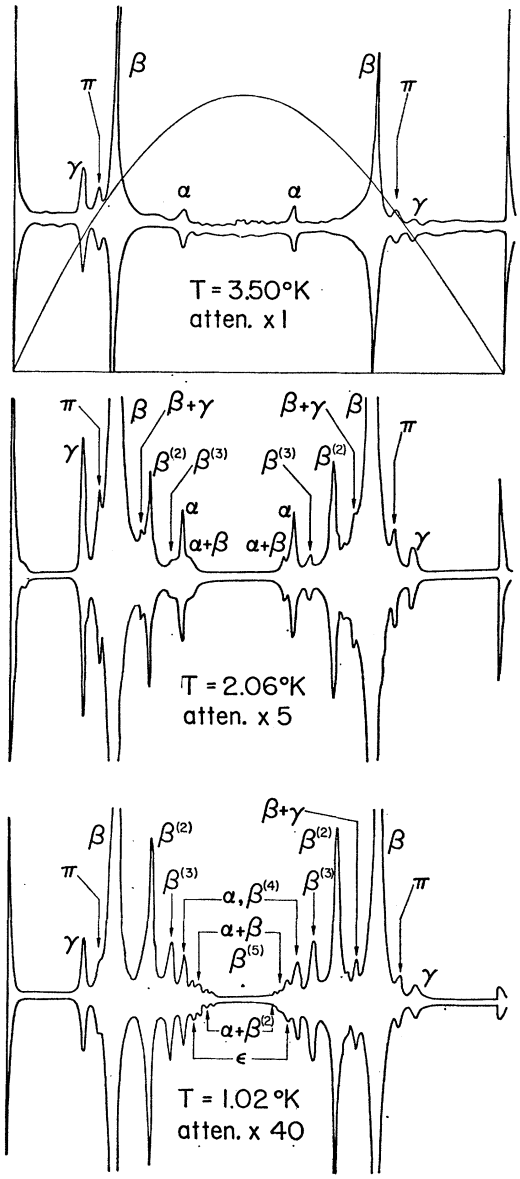

FIG. 1. Envelope spectra of the de Haas–van Alphen periods in lead, as a function of temperature, for the magnetic-field direction along [001]. The profile of the impulsive field was essentially the same for all three discharges, but it is shown only in the top oscillogram for the sake of clarity. Maximum field: 120 kG; sweep time: 16 msec; time-frequency at resonance: 147 kc/sec.

Fermi energy E_f and two Fourier components of the pseudopotential, V_{111} and V_{200}, are regarded as fitting parameters. In a heavy metal such as lead, however, the rather strong spin-orbit interaction would be expected to have a marked effect on the band structure, and it was found that agreement with experiment could be greatly improved when this interaction was allowed for in a phenomenological fashion by the introduction of a fourth fitting parameter, the spin-orbit coupling constant λ.

An approximate fit to the experimental data has already been discussed in a preliminary report of this work.[17] In that report, fewer than four OPW's were used except in the neighborhood of the corners of the Brillouin zone, and approximate values of the two parameters V_{111} and V_{200} were found by fitting to two small areas of cross section of the Fermi surface, whose shapes could be expressed in analytical form; the larger areas were then found by graphical interpolations. It was also shown there that the probable effect of the spin-orbit interaction would be to improve agreement with experiment. In the present paper the dimensions and areas of all of the relevant sections of the Fermi surface have been computed numerically, no graphical constructions were necessary, and a total of eight experimentally determined areas normal to symmetry directions have been used in a least-squares fitting procedure to determine the four parameters E_f, V_{111}, V_{200}, and λ. This paper also contains a much more complete and reliable set of experimental data.

EXPERIMENTAL PROCEDURE

The basic impulsive-field technique for observation of the de Haas–van Alphen effect has been discussed fully elsewhere.[1,19,20] Most of the technical details of the present apparatus (e.g., magnet construction, electronics, etc.) have been described in our earlier report,[17] so that only a brief account of the experimental procedure will be given here.

The lead single crystals were prepared from zone-refined material supplied by Cominco Products Inc. (Grade 69–A). In the early part of this study, the specimens were grown from seed crystals on a horizontal "Kapitza" furnace in which an oblique temperature gradient was set up in order to minimize the misorientations arising from the columnar growth. However, it was later found that crystals prepared by the Czochralski technique of pulling from the melt were of substantially better quality as far as the substructure was concerned, and such crystals were used for the major part of this study. The diameters of the cylindrical crystals ranged from 0.2 to 0.4 mm, and the resistance ratio $\rho_{300°K}/\rho_{1.2°K}$ of the crystals was found to be typically 4×10^4 (the low-temperature resistance values were obtained by extrapolating the transverse magnetoresistance to zero applied field).

The samples were oriented relative to their mountings by conventional back-reflection x-ray techniques,[17] and two methods were used to rotate the sample and pickup coil with respect to the applied field. In some early experiments, a nylon string was used to turn the pickup system from the top of the cryostat, and the angle of rotation was determined by a technique involving the energizing of two pairs of Helmholtz coils outside the cryostat.[17] The string drive was later re-

[19] D. Shoenberg, in *Progress in Low Temperature Physics*, edited by C. J. Gorter (North-Holland Publishing Company, Amsterdam, 1957), Vol. 2, p. 226.

[20] D. Shoenberg, Phil. Trans. Roy. Soc. (London) **A255**, 85 (1962).

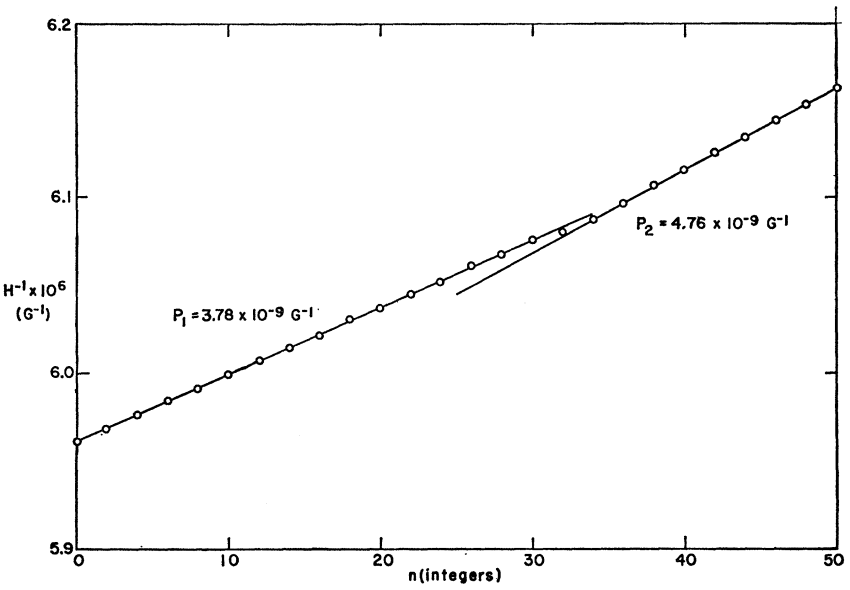

FIG. 2. Typical plot of the values of $1/H$ at cycle maxima versus integers, made in the region where two resonances merge into one another. The periods are given by the slopes of the linear portions.

placed by a bevel-gear device, which had the great advantage of being quite positive and reproducible. Changes in the inclination of the specimens to the applied field could be determined to about $\frac{1}{4}°$, but because of small misalignments of the sample in the pickup system (usually less than 2°), the absolute inclinations were found to an accuracy of about 1° from the symmetries of the angular variations of the de Haas–van Alphen periods. It is believed that the sample could be set to rotate with the field direction always within 3° of any chosen crystallographic plane.

A typical profile of the field pulse is shown at the top of Fig. 1; the highest peak field which could be achieved was 200 kG, and the duration of the pulse was about 16 msec. Because of the many sets of oscillations which are found in lead at high fields, it was essential to use the resonance method[1,20] in order to achieve a satisfactory degree of period separation. The observed resonances were enhanced over and above the natural ones due to the pickup system alone by the use of two electronic band-pass filters, each attenuating at a rate greater than 12 dB per octave above or below the narrow passing band.[21] Figure 1 also shows typical resonance envelopes of the de Haas–van Alphen oscillations when the magnetic field is along a [001] direction. The temperature of the specimen could be varied between 1.0 and 4.24°K, and it can be seen from the figure that the complexity of the oscillograms increases greatly as the temperature is reduced.

In order to achieve maximum accuracy of period measurement, each resonance was expanded until the individual cycles could be resolved, and values of the reciprocal of the field strength at each maximum or minimum were plotted versus integers; for genuine oscillations one should obtain a straight line, and the period is given by its slope. Figure 2 is such an integer plot, made in a region where one resonance gives way to another, and shows two linear regions corresponding to the two periods. As usual, period values from the corresponding expanded resonances on rising and falling fields were averaged in order to minimize various systematic errors,[20] and bucking techniques were used to provide optimum accuracy in the field measurement.[1] The large amount of measuring and data reduction was greatly facilitated by projecting each photograph of the oscillations and the associated field variation onto the screen of a device which would provide analog voltages corresponding to the positions of the field trace and calibration lines; these voltages were automatically transferred to punched cards for computer analysis.

CLASSIFICATION OF THE PERIOD RESULTS

As we shall see later, all of the periods which would be expected on the basis of a nearly-free-electron model should be observable for field directions lying in a {110} plane (which contains the three symmetry directions). For this reason we have concentrated on measuring the period variations in this plane; some results for field directions in other planes are given in Refs. 1 and 17. The angular dependences of all the observed periods in the $(1\bar{1}0)$ plane have been collected and presented on a logarithmic scale in Fig. 3. Each point in the figure is the average of at least two independent measurements for both rising and falling fields; if, for any group of oscillations, more than one point is given for any orientation, then these points refer to results from entirely separate runs and frequently involve different specimens.

Before proceeding with an interpretation of the various terms, it should be realized that not all of the periods in Fig. 3 are fundamental ones. In particular,

[21] Krohn-Hite Corporation, Model 315–*A* (*R*). The low-pass and high-pass sections were usually set at the same cutoff frequency, thereby resulting in the narrowest possible bandwidth.

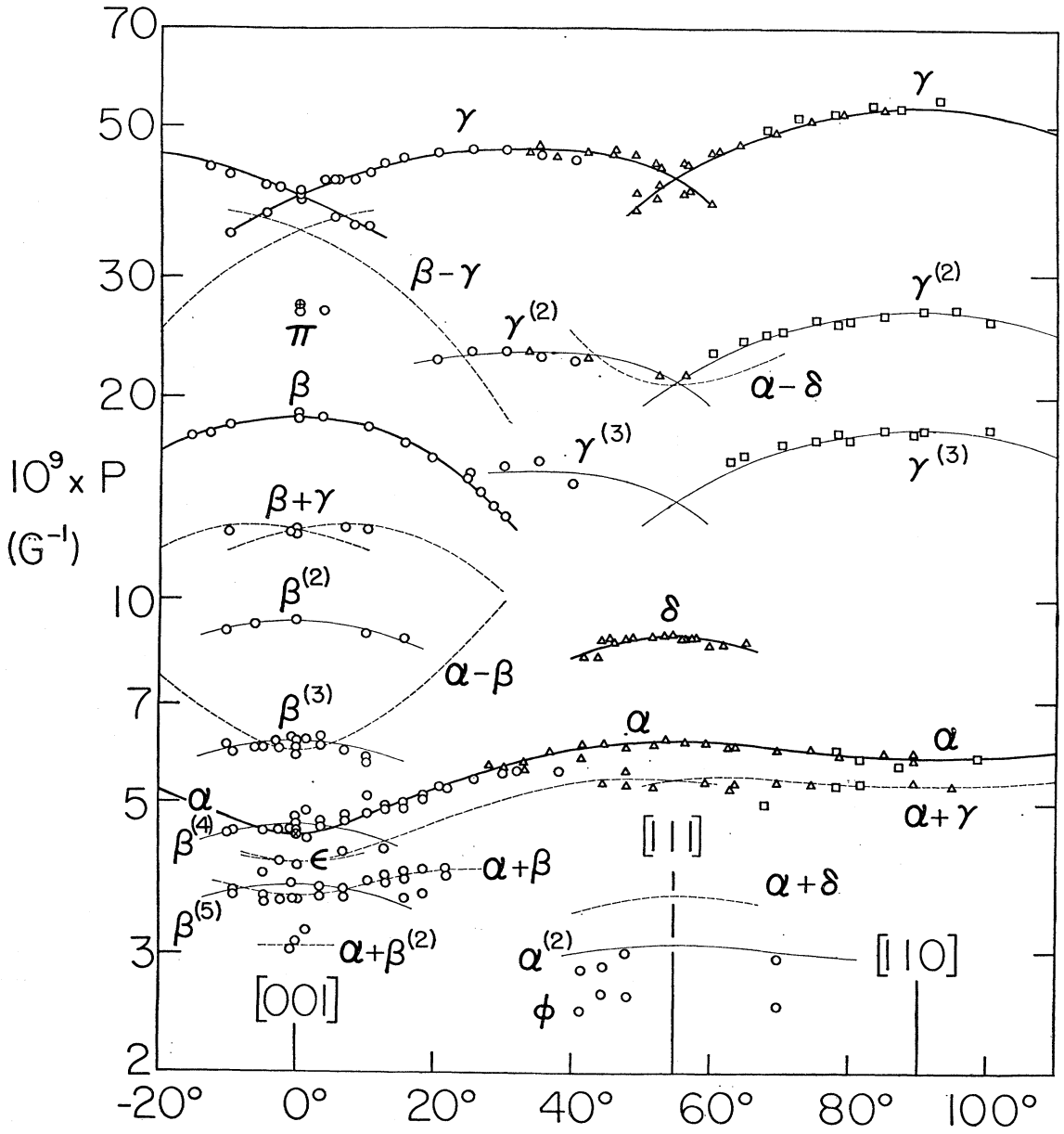

FIG. 3. Angular dependence of all the periods found in lead for magnetic-field directions in the $(1\bar{1}0)$ plane; the periods have been plotted on a logarithmic scale. ○, ⊗, ⊕, [001] crystals at 1.0, 2.0, and 3.5°K, respectively; △, [111] crystals at 1.0°K; □, [110] crystals at 1.0°K. Heavy solid curves: fundamental terms; light solid curves: harmonic terms predicted from fundamental curves; light broken curves: combination terms predicted from fundamental curves.

the exceptionally strong β oscillations are very rich in harmonic content, and from Fig. 1 it can be seen that the fundamental and its retinue of harmonics $\beta^{(2)}$, $\beta^{(3)}$, $\cdots$, etc. completely dominate the low-temperature oscillograms at [001], swamping other fundamental terms of lesser amplitude. The branches α, β, γ, and δ in Fig. 3 are undoubtedly fundamental ones,[22] and heavy curves have been drawn through the points in these branches to satisfy the requirements of crystal symmetry. When drawing the heavy curves through the points for the γ oscillations, it has been assumed that the separate branches cross rather than touch one another at both the [001] and [111] orientations in this plane. It is, in fact, extremely difficult to distinguish experimentally between these two possibilities, since a detailed analysis would require a careful study of the beat patterns near the symmetry directions; however, the resonance technique is required for the very detection of the γ oscilla-

[22] The α, β, and γ oscillations are those which were originally reported in Ref. 1. In that paper, the period variations for the γ oscillations are given for two further planes of rotation; at that time, the α oscillations could be detected with certainty only within about 25° around the [110] direction.

TABLE I. Extremal areas of cross section.

Oscillation orientation	$10^9 P(G^{-1})$ experimental	Interpretation: zone, orbit	$\mathcal{A}_0{}^i((2\pi/a)^2)$ Experimental, from P	4-parameter[a] Fermi surface	Empty-lattice model
α [001]	4.51±0.05	2 ψ_1	1.29 ±0.01[e]	1.2869 (1.2763)	1.792
α [111]	6.17±0.05	2 ψ_1	0.940±0.008[e]	0.9346 (0.9413)	1.097
α [110]	5.94±0.05	2 ψ_1	0.976±0.008[e]	0.9851 (0.9820)	1.141
γ [001]	39.4 ±0.6	3 ζ[c]	0.147±0.002	0.1502	···
γ [111]	42.6 ±0.4	3 ζ	0.136±0.001$_5$[e]	0.1364 (0.1356)	0.183
γ [110]	53.2 ±0.5[b]	3 ζ	0.109±0.001[e]	0.1078 (0.1073)	0.155
π [001]	27.1 ±0.4	3 ξ	0.214±0.003[e]	0.1917 (0.1911)	0.128
β [001]	18.6 ±0.2	3 ν	0.311±0.004[e]	0.3089 (0.3115)	0.322
δ [111]	8.76±0.1$_5$	3 θ	0.66 ±0.01[e]	0.6346 (0.6293)	0.661
ϵ [001]	4.1 ±0.2	3 η	1.41 ±0.07	1.4429 (1.4511)	1.696
ϕ [111]	2.6 ±0.1	3 σ	2.2 ±0.1	2.3035 (2.3021)	2.491
···[110]	···	3 ω	···	0.2380 (0.2378)	0.355
···[110]	···	3 κ[d]	···	~0.68	···
···[110]	···	3 τ[d]	···	~1.86	···

[a] The results in brackets are those obtained by setting the normalization parameter N_p equal to 0.5 rather than to zero (Appendix I).
[b] At [110] the γ oscillations exhibit long beats with 42.5±0.5 cycles per beat, indicating two distinct periods which differ by 2.2%; the two terms have comparable amplitudes since the beat pattern has narrow minima. The value quoted for P is the mean of the two periods.
[c] Nonextremal with respect to $\mathcal{A}$ in the empty-lattice model; the value for $\mathcal{A}_0$ from the 4-parameter model refers to the extremal section which is found to be about $0.04(2\pi/a)$ distant from points K or U.
[d] Nonextremal with respect to $\mathcal{A}$ in both empty-lattice and 4-parameter models.
[e] Areas used in the least-squares fitting procedure.

tions near [001], and this method is not suitable for an accurate determination of beat periods. (Two branches of the γ oscillations were once assumed to touch one another at [001],[1] but we shall see later that our interpretation in terms of a nearly-free-electron model requires that the curves should cross.) Close to [001], the α period can be measured reliably only above about 2.0°K, since at lower temperatures these oscillations are completely masked by the harmonic $\beta^{(4)}$ (see Fig. 1).

In order to demonstrate which of the remaining terms in Fig. 3 are harmonics, thin solid curves have been drawn to represent exact integral submultiples of the periods of the fundamental terms, and it can be seen that many of the period values lie on such harmonic curves. The identification of the harmonics has been further confirmed at symmetry orientations by making rough estimates of the associated effective-mass parameters (from the temperature dependence of the amplitudes), and checking that these are approximately integral multiples of the effective masses for the relevant fundamental terms. In addition to the harmonics, yet further nonfundamental terms are expected on account of the basic nonlinearity of the magnetic properties of the crystal,[20,23] of which the simplest are obtained from sum or difference combinations of the fundamental frequencies. The expected period variations for such terms are shown as the broken curves in Fig. 3, and several of the remaining points are seen to follow some of these dashed curves quite closely; in particular the combination term $\alpha+\beta$ is found to be very strong at 1.0°K and near [001]. A curious feature is that only certain *sum* terms have been found, and in no instance do points appear to follow the broken curves predicted for the *difference* terms; this apparent absence is not yet understood.

We conclude this review of the basic data with a discussion of three groups of low-amplitude oscillations π, ϕ, and ϵ, which are very difficult to measure reliably. The π oscillations have been detected only in the immediate vicinity of [001], and we believe these oscillations to be fundamental ones since they do not appear to fall anywhere into the scheme of either harmonics or of combination tones; the same conclusion would seem to apply to the short-period ϕ oscillations which are found around the [111] direction. The classification of the weak ϵ oscillations near [001] is not, however, so

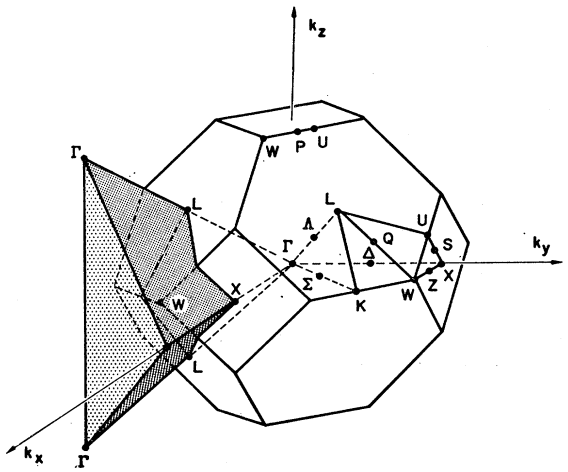

FIG. 4. Primitive Brillouin zone for the fcc structure, showing a tetrahedral cell similar to the one used for the orbit calculations. A smaller cell could have been chosen, but would have been less convenient when tracking large orbits.

[23] A. B. Pippard, Proc. Roy. Soc. (London) A272, 192 (1963).

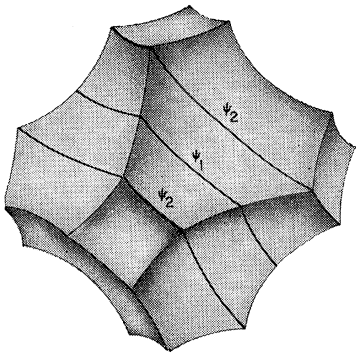

FIG. 5. The empty-lattice hole surface in the second zone (to scale). ψ_1, central [111] extremal orbit; ψ_2, noncentral [111] extremal orbit.

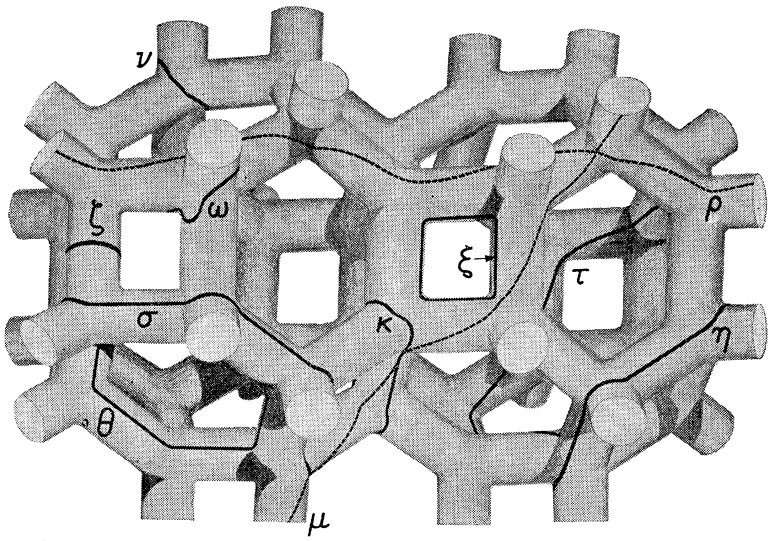

FIG. 6. A portion of the empty-lattice electron surface in the third zone (schematic). The orbits κ and τ are nonextremal with respect to area, and the broken curves depict the open orbits ρ and μ.

straightforward. As can be seen from Fig. 3, the ϵ period values appear to lie on the dashed curve predicted for the $\alpha+\gamma$ combination term; however, if this interpretation were correct, it would be difficult to understand why there should be a lack of experimental points corresponding to the portion of the dashed curve between about 15° and 40°. We shall see later that the model Fermi surface actually leads one to expect a fundamental term with a predicted period close to the ϵ results.

As far as the interpretation of the results in terms of the shape of the Fermi surface is concerned, we shall henceforth consider only the terms α, β, γ, and δ, which are definitely fundamental ones, as well as the three weak terms π, ϕ, and ϵ discussed above; the harmonics and combination tones will not concern us any further. The period values for these seven basic terms at symmetry directions are given in the second column of Table I. The results for the π- and α-oscillations at [001] are from the more reliable measurements at higher temperatures (Fig. 3), and in estimating the reliability of all the results, we have considered not only the scatter of the individual measurements before averaging, but we have also taken into account effects of small misalignments of the specimens by considering the rapidity of the period variations in the neighborhood of the symmetry axes. In the fourth column of Table I we give the associated areas of cross section of the Fermi surface, calculated from the Onsager-Lifshitz-Kosevich relation

$$\mathcal{A}_0 = 2\pi e/chP. \tag{1}$$

The values of $\mathcal{A}_0$ have been expressed in the convenient unit of $(2\pi/a)^2$, where $a=4.90$ Å is the lattice constant of lead at 0°K; the difference between the lattice constant at room temperature 4.94 Å and the value of 0°K has been estimated from thermal-expansion data.[24] Equation (1) then becomes numerically

$$\mathcal{A}_0 = 5.80\times 10^{-9} P^{-1} (2\pi/a)^2. \tag{1a}$$

We now turn to a comparison of the periods of the basic oscillations with the periods calculated from the various areas of cross section of the Fermi surface suggested by the free-electron model; this identification can now be carried out in more detail than was originally done in Ref. 1. Figure 4 shows the primitive Brillouin zone for the fcc structure, with symmetry points and lines labeled according to the notation of Bouckaert *et al.*[25] If we assume that lead may be regarded as having four free electrons per atom, then the empty-lattice model (in which the sole effect of the lattice is to permit Bragg reflections of the electrons, but otherwise leave them completely free) predicts[1,14] a completely filled first zone, a large surface containing unoccupied states in the second zone (Fig. 5), and a multiply connected surface containing occupied states in the third zone (Fig. 6); the model also predicts small electron pockets in the fourth zone, centered on the zone corners W (these pockets are not illustrated). While the empty-lattice hole surface in Fig. 5 has been drawn to scale,[14] the multiply connected electron surface in Fig. 6 has been presented in a simplified schematic fashion, solely for convenience in visualization; the {110} "arms" in the figure have been drawn considerably thinner than in the idealized model.[14]

Most of the orbits shown in Figs. 5 and 6 are typical extremal areas of cross section which would be expected to give rise to de Haas–van Alphen oscillations. We

[24] G. K. White, Phil. Mag. **7**, 271 (1962).
[25] L. Bouckaert, R. Smoluchowski, and E. Wigner, Phys. Rev. **50**, 58 (1936).

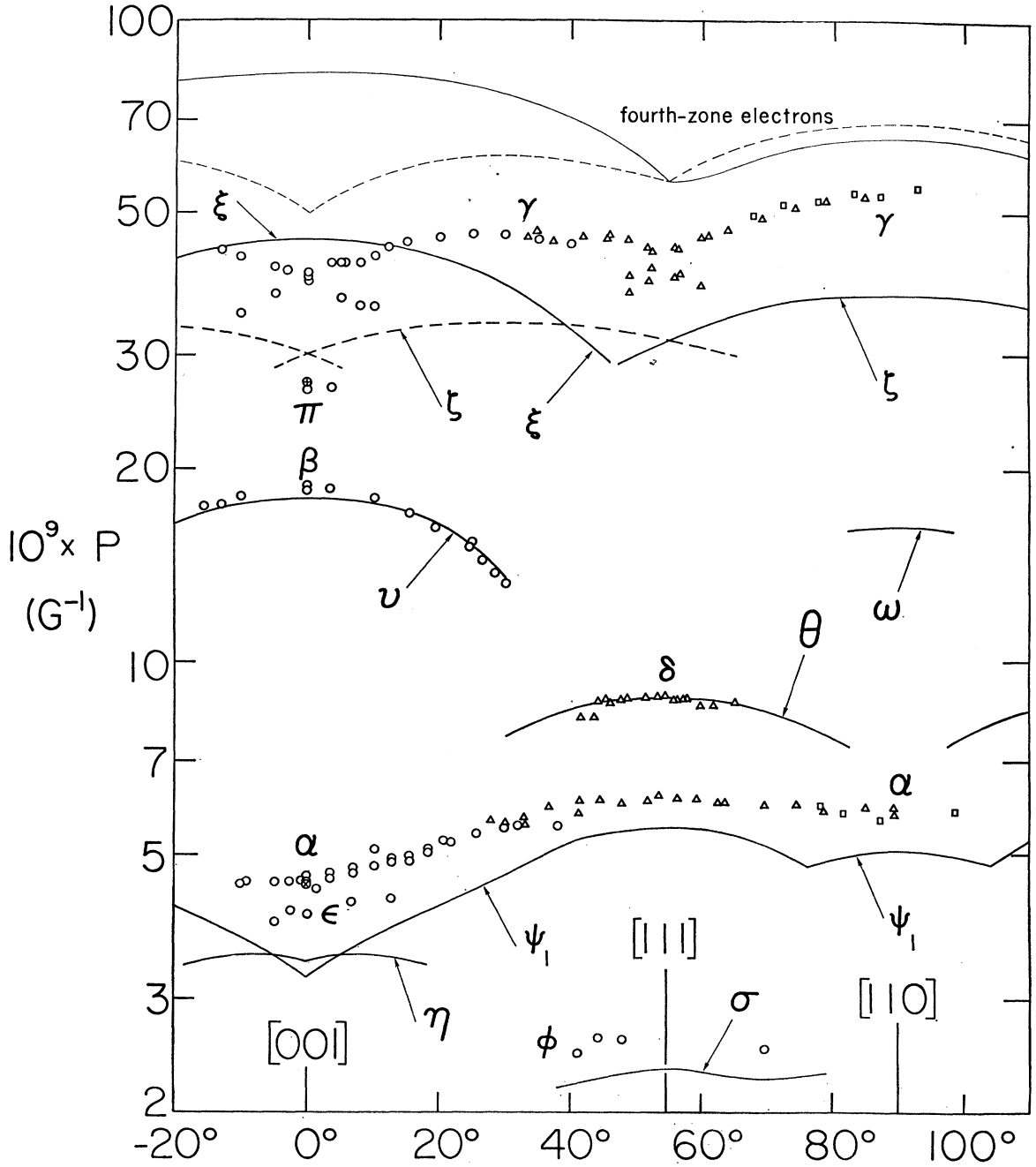

FIG. 7. A comparison of the empty-lattice period variations (arrowed curves) with the fundamental period values from Fig. 3. The broken curves refer to orbits which contain a symmetry point (e.g., W, K, or U) but which need not be extremal with respect to area. The field directions are in the $(1\bar{1}0)$ plane and the periods are plotted on a logarithmic scale; see Fig. 3 for an explanation of the symbols for the experimental points.

have used Harrison's method[26] to find their areas by graphical construction and Eq. (1a) to find the corresponding periods, and the empty-lattice period variations for the $(1\bar{1}0)$ plane are shown in Fig. 7 (arrowed) for comparison with the experimental results. The branches for orbit ζ have been constructed assuming that the plane of the extremal orbit always contains the symmetry point K (or U) for arbitrary orientation of its normal. There is, however, no symmetry requirement that this need be so for two of the branches, and these are distinguished by the dashed curves; in fact according to the literal empty-lattice model there is no extremal area of cross section for type-ζ orbits near [001],[17] but the variation of the area along the direction of the normal does develop a minimum as the lattice

[26] W. A. Harrison, Phys. Rev. 116, 555 (1959).

potential is introduced. Similarly, it has been assumed that all extremal sections through the tetrahedral fourth-zone electron pockets contain the zone corner W, but again this is not required by symmetry for one of the branches.

The most striking features of Fig. 7 are the remarkably close agreements of the empty-lattice periods for orbits ν and θ with the observed β and δ branches, respectively. Also the form of the period variations for orbits ζ and ψ_1 agrees roughly with what is observed for the γ and α oscillations, respectively. Moreover, if we suppose that a weak lattice potential is introduced, this would be expected to have the effect of increasing the number of electrons in the second zone at the expense of electrons in the third zone, and from Eq. (1) we would expect the period curves for both of the orbits ζ and ψ_1 to rise, giving better agreement with experiment. We therefore associate the α oscillations with orbit ψ_1 and the γ oscillations with orbits of type ζ. By similar arguments, the lattice potential would be expected to shrink the fourth-zone electron pockets, thereby raising the associated branches above the empty-lattice ones. However, a careful experimental search has revealed no evidence of periods which are longer than those for the γ oscillations, and this lack of data leads us to conclude that the fourth zone is completely empty. The size of the hole-type orbit ξ on the third-zone surface would be expected to be larger in reality, i.e., of shorter period, and we associate the π oscillations with this orbit even though their range of observation is so limited. Finally, it is possible that the ϵ and ϕ oscillations might be ascribed to orbits η and σ, respectively, although the combination terms and harmonics which occur in these regions make any interpretation difficult, and no evidence has been found for oscillations corresponding to orbit ω. The above interpretation of the experimental results in terms of orbits suggested by the empty-lattice model is summarized in Table I, and the empty-lattice areas of cross section for symmetry directions are given in the last column of the table.

Our interpretation of the strong β oscillations in terms of orbit ν calls for some comment, since these oscillations were originally attributed to the ξ orbit[1]; while the empty-lattice periods for orbits ν and ξ differ in magnitude, the angular variations are actually very similar (Fig. 3). The present assignment is believed to be correct for the following two reasons:

(i) As we have already pointed out, the period values of the β oscillations agree closely with the empty-lattice curve for orbit ν. Introduction of small band gaps improves the over-all agreement with experiment as far as the other orbits are concerned, whereas this good agreement is lost if the β oscillations are associated with orbit ξ instead.[17]

(ii) The effective mass for the β oscillations is found from the temperature dependence of the amplitude to be close to $1.20m_0$ at [001], and a mass parameter having essentially the same value has been found in cyclotron resonance experiments.[7,3,8] When that particular cyclotron resonance is studied at [001] for different microwave polarizations, the results show that the relevant orbit is one for which only the *average* electron velocity in the direction of the magnetic field, $\bar{v}_z$, is zero, while v_z itself is not zero at all points on the orbit. The vanishing of only the average velocity is a property of orbit ν, whereas $v_z=0$ at all points on orbit ξ.

Before leaving the subject of the orbit assignments, we wish to point out that the empty-lattice hole surface in the second zone will also support noncentral extremal orbits ψ_2 in addition to the central ones of type ψ_1 (Fig. 5), and it might well be asked whether the periods labeled $\alpha+\gamma$ in Fig. 3 might not be ascribed to oscillations arising from such noncentral orbits. However, in the final four-parameter model for the actual Fermi surface, which will be shown to account remarkably well for all the other oscillations, the empty-lattice Fermi surface is "sandpapered" to such an extent that no noncentral orbits are possible in reality; this rounding-off is illustrated for areas normal to the [111] direction in Fig. 8. We therefore conclude that the points $\alpha+\gamma$ do indeed represent a combination tone. Also included in Fig. 6 are two further closed orbits κ and τ which are not extremal, and indeed no oscillations have been found which could reasonably be ascribed to them.

To sum up, we have seen that the empty-lattice model with four free electrons per atom appears to be a reasonable approximation to the actual Fermi surface. However, this is perhaps surprising when one considers that there is a sizeable energy gap of about 0.7 Ry between the $6s$ and $6p$ states in the free lead atom.[27] In the lead salts, the $6s^2$ electrons frequently appear to behave as an "inert pair" of core electrons, and one might ask whether or not a model based on the assumption of only two ($6p^2$) electrons would be equally satisfactory. However, a nearly-free-electron model with only two electrons per atom does not predict, in particular, a single large hole surface in the second zone,[14] and it would not be possible to account for the observed branch of short-period α oscillations. The ultimate success of the four-electron model will become apparent in detail after our final four-parameter calculation, in which the parameters are found to have values which are physically reasonable. However, we might point out at this stage that further confidence in the model can be obtained from a consideration of the sections in the extended- and reduced-zone schemes which are formed by the intersection of the Fermi surface with the central [110] plane through Γ (Figs. 9 and 10). Irrespective of the detailed shape of the Fermi surface, the total occupied area in the extended-zone scheme of Fig. 10 is given by

$$\mathcal{A}_{[110]}{}^{\mathrm{ext}}=2\mathcal{A}_{[110]}{}^{\mathrm{Bz}}+2\mathcal{A}(\zeta_{[110]})-\mathcal{A}(\psi_{1,[110]}),$$

[27] F. Herman and S. Skillman, *Atomic Structure Calculations* (Prentice-Hall, Inc., Englewood Cliffs, New Jersey, 1963).

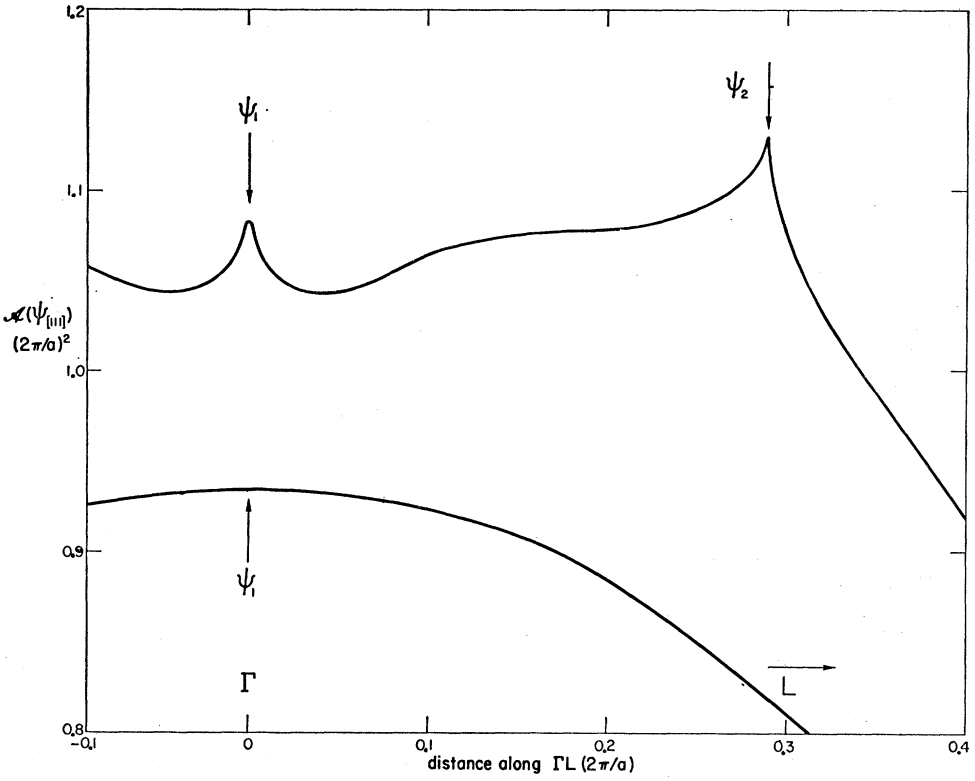

FIG. 8. Variation of the [111] area of cross-section of the second-zone hole surface as a function of the normal distance from the zone center Γ. Upper curve: empty-lattice model; lower curve; model Fermi surface, with the parameter values given in Eq. (30). ψ_1 and ψ_2 refer to the orbits shown in Fig. 5.

where $\mathcal{A}_{[110]}{}^{\mathrm{Bz}}$ is the central cross-sectional area of the Brillouin zone normal to [110]; a similar expression holds for the central slice normal to [111]. For a four-electron sphere, the area of the diametral cross section is $\mathcal{A}_0{}^{\mathrm{fe}}=4.832(2\pi/a)^2$, and from the areas deduced from the periods of the γ and α oscillations (Table I) we find

$$\mathcal{A}_{[110]}{}^{\mathrm{ext}}=(1.01\pm0.01)\mathcal{A}_0{}^{\mathrm{fe}}$$

and

$$\mathcal{A}_{[111]}{}^{\mathrm{ext}}=(0.99\pm0.01)\mathcal{A}_0{}^{\mathrm{fe}}.$$

Thus, within experimental error, these total areas are indistinguishable from the diametral area of the Fermi surface for four completely free electrons per atom. We might also mention that positron annihilation experiments also support our model.[28] Later on we shall calculate the band structure $E(\mathbf{k})$ using the experimentally determined parameters, and it will be shown that the energy bands do indeed reflect something of an inert-pair behavior in the metal; however the $6s$-like band is by no means narrow, and thus it would appear to be wrong to regard the $6s^2$ electrons as localized.

CALCULATION OF THE FERMI SURFACE

Having established that the empty-lattice model can account qualitatively for the experimental results, we now proceed with a quantitative calculation of the shape of the actual Fermi surface. To do this, we make use of an interpolation scheme which is similar to that suggested by Harrison[13] and which is based on the pseudopotential concept.[12,15] In this approach the ordinary lattice potential $V(\mathbf{r})$ is replaced by a weak pseudopotential, which is actually a complicated integral operator containing terms which result from the orthogonalization of the crystal wave function to the occupied core states $1s$, $2s$, $\cdots$, $5d$, as well as exchange terms. In the interpolation scheme used here, the nonlocal pseudopotential is replaced by an ordinary function of coordinates, and to introduce the notation, as well as for the sake of clarity, we give first a brief outline of the method when the spin-orbit coupling can be ignored.

We follow closely the Phillips-Kleinman approach[12] and introduce functions ϕ to represent the "smooth" parts of the crystal wave functions χ; new functions ψ are then constructed from the ϕ's by orthogonalization to the core states, and each χ is expanded in terms of the new basis set ψ,

$$\chi_{\mathbf{k}}=\sum_{\kappa} C_{\kappa}{}^{\mathbf{k}}\psi_{\kappa}{}^{\mathbf{k}}, \tag{2}$$

where $\boldsymbol{\kappa}$ is a reciprocal-lattice vector. When the simplified pseudopotential $V^p(\mathbf{r})$ is expressed as a Fourier series

$$V^p(\mathbf{r})=\sum_{\kappa} V_{\kappa}e^{i\kappa\cdot\mathbf{r}}, \tag{3}$$

and the smooth functions ϕ are taken to be plane waves (i.e., the crystal wave functions are expressed as linear combinations of OPW's), the Schrödinger equa-

[28] A. T. Stewart, Can. J. Phys. **35**, 168 (1957).

tion yields the set of coupled equations

$$T(\mathbf{k}-\boldsymbol{\kappa})C_{\kappa}^{\mathbf{k}}+\sum_{\kappa'} C_{\kappa'}^{\mathbf{k}}V_{\kappa'-\kappa}=E(\mathbf{k})C_{\kappa}^{\mathbf{k}}, \quad (4)$$

in which the matrix elements of the kinetic energy are given by

$$T(\mathbf{k}-\boldsymbol{\kappa})=(\hbar^2/2m)(\mathbf{k}-\boldsymbol{\kappa})^2. \quad (5)$$

With these approximations the Eqs. (4) reduce formally to those for the classic plane-wave expansion (Sommerfeld and Bethe[29]). We now assume that higher Fourier components of the pseudopotential are negligibly small and that only a few components with small $|\boldsymbol{\kappa}|$ are required to fit the experimental results, with the V_{κ} regarded as adjustable parameters. Although fewer than four OPW's are sufficient to resolve the empty-lattice degeneracies at most points in the Brillouin zone, at least four are required at the zone corners W. Awkward graphical interpolations[17] can be avoided if four OPW's are used for each wave vector $\mathbf{k}$ and with this choice the resultant Hamiltonian matrix from Eqs. (4) becomes truncated to

$$\mathcal{H}_l=\begin{bmatrix} T(\mathbf{k}) & V_{200} & V_{111} & V_{111} \\ V_{200} & T(\mathbf{k}-\boldsymbol{\kappa}_2) & V_{111} & V_{111} \\ V_{111} & V_{111} & T(\mathbf{k}-\boldsymbol{\kappa}_3) & V_{200} \\ V_{111} & V_{111} & V_{200} & T(\mathbf{k}-\boldsymbol{\kappa}_4) \end{bmatrix}, \quad (6)$$

where a typical set of reciprocal-lattice vectors for the fcc structure is, in units of $(2\pi/a)$,

$$\boldsymbol{\kappa}_1\equiv 0, \quad \boldsymbol{\kappa}_2=(0,0,2), \quad \boldsymbol{\kappa}_3=(1,1,1), \quad \boldsymbol{\kappa}_4=(1,-1,1). \quad (7)$$

Of course, more than four OPW's could be used, but then the essential simplicity of the model would be lost. This four-OPW model with a local pseudopotential is the same as that used by Harrison[13] and by Ashcroft.[18]

The secular equation resulting from the use of the Hamiltonian (6) may be formally written as

$$F\{E(\mathbf{k}),V_{111},V_{200},\mathbf{k}\}=0, \quad (8)$$

and the zeros of the polynomial F were found as a function of $\mathbf{k}$ for fixed values of $E(\mathbf{k})$, V_{111}, and V_{200} by a computer calculation. In this manner, surfaces of constant energy could be traced out in $\mathbf{k}$ space; the intersections of these surfaces with symmetry planes determined the cross-sectional areas corresponding to the various closed orbits in different bands. In fitting to the observed areas (Table I), we have regarded the Fermi energy E_f as a third fitting parameter, and have set $E(\mathbf{k})=E_f$. One of the zone corners, W_a say, was taken to be the center of a calculation region, a tetrahedral cell bounded by the {110} planes which bisect the lines joining W_a to its four nearest equivalent neighbors, W_b say; such a cell is shown in Fig. 4. Only those reciprocal-lattice vectors $\boldsymbol{\kappa}_i(i=2,3,4)$ corresponding to Bragg planes intersecting at W_a are included in the Hamiltonian matrix (6), and the vectors given in Eqs. (7) are those appropriate to the cell centered on the zone corner $(\frac{1}{2},0,1)(2\pi/a)$. However, for a point $\mathbf{k}$ lying in one of the adjacent elementary tetrahedra corresponding to one of the corners W_b, the function F had to be changed by replacing the $\boldsymbol{\kappa}_i$ used for W_a by those appropriate to that particular W_b, and so forth. The calculation was programmed so that such changes were effected automatically, and in this manner orbits on a constant-energy surface could be followed continuously. The details of the procedures used in these computations are given elsewhere.[30]

When preliminary calculations were carried out with just three fitting parameters E_f, V_{111}, and V_{200}, reasonably accurate fits to the second-band hole surface and to the third-band electron surface could not be achieved simultaneously; in fact, when a good fit was made to orbits on one surface, a mismatch of typically 5 or 6% was found between the calculated and experimental areas for the other surface. It seems unlikely that the inclusion of higher order V_{κ} would improve the agreement for the following reason. We note that, in the empty-lattice model with four electrons per atom, the region of occupied states does not extend very far beyond the fundamental Brillouin zone. Even if the higher order V_{κ} were to have magnitudes similar to V_{111} and V_{200}, they would be expected to contribute little to the energy on account of the large energy denominators in second-order perturbation theory. (Actually, interactions with higher states are included to second order in the experimentally determined parameters V_{111} and V_{200}.[31]) On the other hand, it is well known that relativistic effects become important in heavy elements, and to seek a better description of the Fermi surface it seemed desirable to take into account the simplest of the relativistic terms, the spin-orbit interaction.

The spin-orbit coupling term in the Hamiltonian has the form[32]

$$\Omega=(\hbar/4m^2c^2)(\boldsymbol{\nabla}V\times\mathbf{P})\cdot\boldsymbol{\sigma}, \quad (9)$$

where $V(\mathbf{r})$ is the actual potential seen by the electron, $\mathbf{P}$ is the momentum operator, and the components of $\boldsymbol{\sigma}$ are the Pauli spin matrices. For free atoms, Eq. (9) reduces to

$$\Omega^a=(1/2m^2c^2)((1/r)(dV/dr))\mathbf{l}\cdot\mathbf{s}=\xi(r)\mathbf{l}\cdot\mathbf{s}, \quad (10)$$

and it is customary to characterize the strength of the interaction by the one-electron atomic parameter

$$\xi_{nl}=\hbar^2\int_0^{\infty} R_{nl}^2(r)\xi(r)r^2dr, \quad (11)$$

where R_{nl} is the radial part of the wave function; for lead the atomic parameter ξ_{6p} is quite large, namely

[29] A. Sommerfeld and H. Bethe, *Handbuch der Physik*, edited by H. Geiger and Karl Scheel (Julius Springer, Berlin, 1933), Vol. 24(2), p. 333.

[30] J. R. Anderson and M. K. Rhyne, U. S. Atomic Energy Commission Report IS-1106 (unpublished).

[31] M. H. L. Pryce, Proc. Phys. Soc. (London) **A63**, 25 (1950).

[32] Cf: H. Jones, *Theory of Brillouin Zones and Electronic States in Crystals* (North-Holland Publishing Company, Amsterdam, 1960), Chap. 7.

0.066 Ry.[33] When the spin-orbit interaction is included in the pseudopotential formalism, the Eqs. (4) must be modified to read

$$T(\mathbf{k}-\boldsymbol{\kappa})C_{\kappa}^{\mathbf{k}}+\sum_{\kappa'}C_{\kappa'}^{\mathbf{k}}V_{\kappa'-\kappa}+\sum_{\kappa'}C_{\kappa'}^{\mathbf{k}}\Omega_{\kappa',\kappa}^{\mathbf{k}} =E(\mathbf{k})C_{\kappa}^{\mathbf{k}}. \quad (12)$$

As in Eqs. (4), the kinetic-energy and pseudopotential matrix elements refer to the plane waves ϕ, whereas the spin-orbit matrix elements are evaluated using the OPW's ψ; since we have been using four OPW's for each point $\mathbf{k}$ in the absence of the spin-orbit interaction, a total of eight will be required when the spin is taken into account. Because Ω depends on the potential gradient [Eq. (9)], we should expect that the main contributions to the spin-orbit terms will come from regions near the ion cores. In such regions we assume that the OPW's will resemble quite closely the wave functions $6s$, $6p$, $\cdots$, for the free atom, and the potential $V(\mathbf{r})$ will be approximately spherically symmetrical about each nucleus. In order to determine the form of the spin-orbit interaction for metallic lead, it should thus be a reasonable approximation to treat the actual wave functions as linear combinations of $6s$ and $6p$ atomic functions, and we shall neglect all states of higher angular momentum ($6d,\cdots$); however, the relative strengths of the s and p contributions are not known *a priori*. We therefore introduce a phenomenological spin-orbit constant λ which contains all the radial dependence in the spin-orbit matrix element; while λ takes the same form as ξ_{6p}, it will be regarded here as a fourth fitting parameter.

In order to explain our final choice of a basis set of wave functions, we consider first the regime at a zone corner W, the center of our calculation cell. The points W are of particular interest since the empty-lattice Fermi surface in any band is always close to one of these symmetry points. Furthermore, it can be shown that, for the nearly-free-electron model, the energy in the fourth band always has a local minimum at W (at least for $\lambda=0$), and we wish to impose upon our final model the experimental requirement that the fourth band be empty; in the three-parameter model, the Fermi level was found to be only barely below the minimum. It is thus important that the wave functions at W be chosen properly. Moreover, the formalism at W is particularly simple since symmetry requires that the s-p wave functions at this point be either s-like or p-like, but not mixed.[34] In the absence of spin-orbit coupling, consider the following combinations of the four OPW's ψ_i

$$\begin{aligned}&\psi_1'=\tfrac{1}{2}(\psi_1+\psi_2+\psi_3+\psi_4), \quad \psi_3'=\frac{1}{\sqrt{2}}(\psi_1-\psi_2),\\ &\psi_2'=\tfrac{1}{2}(\psi_1+\psi_2-\psi_3-\psi_4), \quad \psi_4'=\frac{1}{\sqrt{2}}(\psi_3-\psi_4).\end{aligned} \quad (13)$$

At any point W these combinations result in pure s and pure p functions, and for the particular zone corner $(\frac{1}{2},0,1)$ we demonstrate the symmetries explicitly by writing

$$\begin{aligned}&\psi_1'\sim\psi_s, \quad \psi_2'\sim\psi_{p_x},\\ &\psi_3'\sim\psi_{p_z}, \quad \psi_4'\sim\psi_{p_y}.\end{aligned} \quad (14)$$

These symmetries can be easily verified by supposing that the ψ_i may be replaced by simple plane waves $\exp\{i(\mathbf{k}-\boldsymbol{\kappa}_i)\cdot\mathbf{r}\}$; we set $\mathbf{k}=\mathbf{k}_W=(\frac{1}{2},0,1)(2\pi/a)$ and the appropriate $\boldsymbol{\kappa}_i$ are given in Eq. (7). The functions ψ_3' and ψ_4' are degenerate; they may be transformed into one another by particular operations of the group of $\mathbf{k}$ at W.[35] For this reason, any linear combinations of ψ_3' and ψ_4' would be equally satisfactory.

When spin is taken into account we consider the eight functions

$$\Phi_m=\psi_i\alpha_j \ (i=1,\cdots 4;\, j=1,2;\, m=i+2[(-1)^i+1]), \quad (15)$$

where α_j is a spinor. There are evidently several natural directions along which the spin could be quantized, and we choose the direction parallel to k_z for the sake of definiteness. At W there are two irreducible representations of the double group, W_6 and W_7, and a correct basis set must contain each of these irreducible representations twice. We now use the zero-spin set (13) as a guide, and construct the set Φ' given by

$$\begin{aligned}&\Phi_1'=\tfrac{1}{2}(\psi_1+\psi_2+\psi_3+\psi_4)\alpha_1,\\ &\Phi_2'=\tfrac{1}{2}[(\psi_1-\psi_2)\alpha_2+i(\psi_3-\psi_4)\alpha_1],\\ &\Phi_3'=\tfrac{1}{2}(\psi_1+\psi_2-\psi_3-\psi_4)\alpha_1,\\ &\Phi_4'=\tfrac{1}{2}[-(\psi_1-\psi_2)\alpha_2+i(\psi_3-\psi_4)\alpha_1],\\ &\Phi_5'=\tfrac{1}{2}(\psi_1+\psi_2+\psi_3+\psi_4)\alpha_2,\\ &\Phi_6'=\tfrac{1}{2}[-(\psi_1-\psi_2)\alpha_1-i(\psi_3-\psi_4)\alpha_2],\\ &\Phi_7'=\tfrac{1}{2}(\psi_1+\psi_2-\psi_3-\psi_4)\alpha_2,\\ &\Phi_8'=\tfrac{1}{2}[(\psi_1-\psi_2)\alpha_1-i(\psi_3-\psi_4)\alpha_2];\end{aligned} \quad (16)$$

at W the functions Φ_1', Φ_2', Φ_5', and Φ_6' belong to W_6 and the others belong to W_7. The set Φ' is formally related to the initial set Φ by the similarity transformation

$$\Phi'=S\Phi, \quad (17)$$

where the 8×8 matrix S is given in Appendix I; the similarity transformation used for the wave functions will, of course, also change the matrix elements in Eq. (12). It should be pointed out that the basis set (16) is by no means unique. The above choice turns out to be convenient since it leads to the correct form for the spin-orbit terms not only at W but also over the entire plane $k_z=2\pi/a$ (square face of the Brillouin zone); moreover, the use of the set (16) also results in a particularly simple spin-orbit Hamiltonian [block-diagonal matrix in Eq. (20)].

We have already assumed for our simplified pseudopotential that the matrix elements V_{κ} are independent

[33] E. U. Condon and G. H. Shortley, *The Theory of Atomic Spectra* (The Macmillan Company, New York, 1935).
[34] Cf. Chap. 3 of Ref. 32.
[35] Cf: G. F. Koster, *Solid State Physics*, edited by F. Seitz and D. Turnbull (Academic Press Inc., New York, 1957), Vol. 5, p. 173.

of $\mathbf{k}$, and we now make a similar assumption for the spin-orbit terms, namely, that the results calculated at W using a proper basis set (16) for this point will be valid for all other points in the Brillouin zone; this simplification is discussed in Appendix I. To find the form of the spin-orbit matrix elements at W we now use Eqs. (13) and (14) to express the functions (16) in a manner which will reflect the atomic-like character of the OPW's in the core region. We then have, again explicitly for the zone corner $(\frac{1}{2},0,1)$,

$$\begin{aligned}
&\Phi_1' \rightarrow N_1\psi_s\alpha_1, \quad && \Phi_2' \rightarrow N_2(\psi_{p_y}\alpha_1+i\psi_{p_z}\alpha_2),\\
&\Phi_3' \rightarrow iN_3\psi_{p_x}\alpha_1, && \Phi_4' \rightarrow N_2(\psi_{p_y}\alpha_1-i\psi_{p_z}\alpha_2),\\
&\Phi_5' \rightarrow N_1\psi_s\alpha_2, && \Phi_6' \rightarrow N_2(-\psi_{p_y}\alpha_2-i\psi_{p_z}\alpha_1),\\
&\Phi_7' \rightarrow iN_3\psi_{p_x}\alpha_2, && \Phi_8' \rightarrow N_2(-\psi_{p_y}\alpha_2+i\psi_{p_z}\alpha_1),
\end{aligned} \tag{18}$$

where the N_i are unknown normalization coefficients. The matrix elements for spherically symmetrical $V(r)$ may be written in the form

$$\langle\Phi_n'|\Omega|\Phi_{n'}'\rangle=\langle\Phi_n'|f(r)\mathbf{l}\cdot\mathbf{s}|\Phi_{n'}'\rangle=\lambda\langle\varphi_n'|\mathbf{l}\cdot\mathbf{s}|\varphi_{n'}'\rangle, \tag{19}$$

in which the radial integration has been absorbed into the phenomenological constant λ [compare Eq. (19) with Eqs. (10) and (11) for the free atom], and the functions φ' are the angular and spin parts of the functions Φ'. When the elements (19) are evaluated in the representation (18), the spin-orbit matrix is found to be of block-diagonal form

$$\mathfrak{IC}_{so}'=\begin{pmatrix} A_{so} & 0 \\ 0 & A_{so}^* \end{pmatrix}, \tag{20}$$

where

$$A_{so}=\frac{\lambda}{2}\begin{bmatrix} 0 & 0 & 0 & 0 \\ 0 & 2N_2^2 & 0 & 0 \\ 0 & 0 & 0 & -2N_2/N_3 \\ 0 & 0 & -N_3/N_2 & -2N_2^2 \end{bmatrix}; \tag{20a}$$

A_{so} is real when evaluated at W, but would be complex in general (Appendix I), and in order that A_{so} be Hermitian, it is necessary to set $2N_2/N_3=N_3/N_2$. We now take the p functions to be normalized over some appropriate volume and set $N_2^2=\frac{1}{2}$ for the sake of definiteness, i.e., we assume $N_2=\sqrt{2}/2$ and $N_3=1$.

In order to determine the total Hamiltonian matrix at any point $\mathbf{k}$ in the Brillouin zone, the lattice Hamiltonian $\mathfrak{IC}_l$ [Eq. (6)] must be transformed into a form appropriate to the set of eight basis functions (16) and then combined with the spin-orbit matrix $\mathfrak{IC}_{so}'$ [Eq. (20)]. The required transformation for $\mathfrak{IC}_l$ is

$$\mathfrak{IC}_l'=S\begin{bmatrix} \mathfrak{IC}_l & 0 \\ 0 & \mathfrak{IC}_l \end{bmatrix}S^{-1} \tag{21}$$

and the total Hamiltonian matrix is then finally given by

$$\mathfrak{IC}_t'=\mathfrak{IC}_{so}'+\mathfrak{IC}_l'=\begin{bmatrix} (A_{so}+A_1) & B_1 \\ -B_1 & (A_{so}+A_1)^* \end{bmatrix}, \tag{22}$$

where

$$A_{so}+A_1=\begin{bmatrix}
U_0+V_{200}+2V_{111} & \frac{i(U_4-U_3)}{4} & \frac{U_1+U_2-U_3-U_4}{4} & \frac{i(U_4-U_3)}{4} \\
\frac{-i(U_4-U_3)}{4} & U_0-V_{200}+\lambda/2 & \frac{i(U_4-U_3)}{4} & \frac{-U_1-U_2+U_3+U_4}{4} \\
\frac{U_1+U_2-U_3-U_4}{4} & \frac{-i(U_4-U_3)}{4} & U_0+V_{200}-2V_{111} & \frac{-i(U_4-U_3)}{4}-\sqrt{2}\lambda/2 \\
\frac{-i(U_4-U_3)}{4} & \frac{-U_1-U_2+U_3+U_4}{4} & \frac{i(U_4-U_3)}{4}-\sqrt{2}\lambda/2 & U_0-V_{200}-\lambda/2
\end{bmatrix} \tag{23}$$

and

$$B_1=\frac{(U_2-U_1)}{4}\begin{bmatrix} 0 & 1 & 0 & -1 \\ -1 & 0 & -1 & 0 \\ 0 & 1 & 0 & -1 \\ 1 & 0 & 1 & 0 \end{bmatrix}. \tag{24}$$

In the above matrices

$$U_i=(\hbar^2/2m)|\mathbf{k}+\boldsymbol{\kappa}_i|^2, \quad i=1,2,3,4, \tag{25}$$

$$U_0=(\hbar^2/2m)\sum_{i=1}^{4}U_i/4, \tag{26}$$

and the $\boldsymbol{\kappa}_i$ are given in Eq. (7). Since the spin-orbit interaction cannot remove the Kramers degeneracy of the energy levels in the independent-particle model, the eigenvalues of the 8×8 Hamiltonian matrix (22) must always occur in four degenerate pairs. While we have not been able to transform the total Hamiltonian into a

simple block-diagonal matrix, the simple form of the submatrix B_1 enables the secular equation to be factored by standard determinantal operations into two identical terms, each containing the determinant of only a 4×4 matrix. This factoring did not introduce any simplications as far as the formal statement of the problem was concerned, but it did result in a substantial reduction in the time required for computer calculations.

The surfaces of constant energy were calculated from the secular equation

$$G\{E(\mathbf{k}),V_{111},V_{200},\lambda,\mathbf{k}\}=0 \tag{27}$$

in the same manner as for the three-parameter model (see Appendix II), and the following physical considerations were taken into account in order to limit the many possibilities in initial trial-and-error fitting calculations. It would seem reasonable to suppose that $\lambda\sim\xi_{6p}$ and also that $E_f\sim E_f^{(0)}$, the free-electron Fermi energy. As far as the pseudopotential coefficients are concerned, a discussion of the ordering of the energy levels is helpful. At W all combinations of the U_i ($i=1, 2, 3, 4$) vanish in Eqs. (23) and (24), and the eigenvalues relative to the empty-lattice energy $(5/4)(\hbar^2/2m)(2\pi/a)^2$ are readily found to be

$$\begin{aligned}
&E_1(W)=2V_{111}+V_{200},\\
&E_2(W)=-V_{111}-\lambda/4-\{(V_{200}-V_{111}+\lambda/4)^2+\lambda^2/2\}^{1/2},\\
&E_3(W)=-V_{200}+\lambda/2,\\
&E_4(W)=-V_{111}-\lambda/4+\{(V_{200}-V_{111}+\lambda/4)^2+\lambda^2/2\}^{1/2}.
\end{aligned} \tag{28}$$

The level $E_1(W)$ is the s-like level $W_6(W_1)$ and is independent of λ. It is reasonable to expect this level to be the lowest of the four because of the large s-p splitting in the free atom; for $\lambda=0$ it is easy to see that this condition requires V_{111} to be negative, a conclusion which remains valid even for $\lambda\neq0$ if we make reasonable choices for the values of the parameters. Moreover, a negative choice for V_{111} causes the energy of the uppermost level $E_4(W)$ to increase when spin-orbit coupling is introduced, i.e., the minimum energy in the fourth zone is raised, thereby ensuring that this band remains unoccupied. Little can be predicted in advance about the sign of V_{200}, but preliminary estimates gave decidedly better fits to the experimental data when both V_{111} and V_{200} were taken to be negative.

The four parameters were determined by a least-squares fit to the areas of eight of the major symmetry orbits. The particular orbits used are denoted by asterisks in Table I; they were chosen not only to give a good representation of the Fermi surface in both the second and third zones but also because the associated period values were the most reliable. Values of E_f, λ, V_{111}, and V_{200} were chosen to minimize the sum of the squares of the weighted deviations

$$Q=\sum_{i=1}^{8}[\mathcal{A}_{\mathrm{calc}}{}^i(E_f,\lambda,V_{111},V_{200})-\mathcal{A}_{\mathrm{exp}}{}^i]^2/(\delta\mathcal{A}^i)^2, \tag{29}$$

where the $\delta\mathcal{A}^i$ are the uncertainties in the experimentally-determined areas (Table I). In a preliminary calculation, Q was evaluated at points on a coarse grid in the four-dimensional $(E_f,\lambda,V_{111},V_{200})$ space, and the position of minimum Q was found approximately by rough graphical interpolation. The point thus found was then used as a starting point for a linear least-squares iteration calculation which is described in Appendix II, and the iterations were carried out until the minimum in Q was located with a precision which was compatible with the accuracy of the experimental information. The point $Q_{\min}$ was demonstrated to be an absolute minimum in the four-dimensional space; second derivatives of Q were evaluated at this point and they confirmed a positive-definite quadratic form.[36] The final values of the parameters at $Q_{\min}$ are, in rydbergs,

$$\begin{aligned}
&V_{111}=-0.084\pm0.002, \quad E_f=0.718\pm0.001 \quad (E_f^{(0)}=0.7079),\\
&V_{200}=-0.039\pm0.002, \quad \lambda=0.096\pm0.002 \quad (\xi_{6p}=0.066),
\end{aligned} \tag{30}$$

and these parameters completely specify the shape of the Fermi surface within the framework of our model; a discussion of the uncertainties quoted above will be deferred until later (Appendix II).

In Fig. 9 we compare the shapes of the various symmetry orbits calculated from the model Fermi surface (heavy curves) with the corresponding empty-lattice sections (circular arcs). The combined effects of the lattice potential and spin-orbit coupling are seen to result in a rounding-off of the sharp corners, but otherwise the calculated and empty-lattice shapes are very similar. The principal differences are also apparent in Fig. 10, in which we show the central [110] section through the Fermi surface in the extended-zone scheme; the model Fermi surface lies remarkably close to the free-electron sphere except near the intersections with the Bragg planes.

Although the values of the parameters λ, V_{111}, and V_{200} given by Eqs. (30) may have little significance for energies other than E_f, we have nevertheless used them to compute the eigenvalues $E(\mathbf{k})$ of the Hamiltonian (22) along principal directions in $\mathbf{k}$ space. The ensuing energy bands are shown in Fig. 11, and the energy levels

TABLE II. Energy eigenvalues at symmetry points (Ry).

Point	E_1	E_2	E_3	E_4
Γ	−0.0138	1.3169	1.4297	1.8771
W	0.3693	0.5392	0.6630	0.7335
X	0.3623	0.4943	0.9149	0.9945
K, U	0.3541	0.5249	0.6410	1.0155
L	0.2397	0.4282	1.1938	1.3652

$V_{111}=-0.0841$ Ry, $V_{200}=-0.0387$ Ry,
$E_f=0.7180$ Ry, $\lambda=0.0961$ Ry.

[36] Cf. T. Apostol, *Mathematical Analysis* (Addison-Wesley Publishing Company, Reading, Massachusetts, 1957).

at the principal symmetry points are listed in Table II. The most striking feature of Fig. 11 is the distinct gap between the filled lowest band, in which the wave functions have predominantly s-like symmetry, and the lowest branch of the p-like bands. For any $\mathbf{k}$, the gap is never less than 0.13 Ry and, as we have pointed out earlier, it is a reflection in the metal of the large s-p splitting in the free atom ("inert-pair" behavior). One major effect of the spin-orbit coupling is to split the otherwise degenerate level W_3 into the two levels

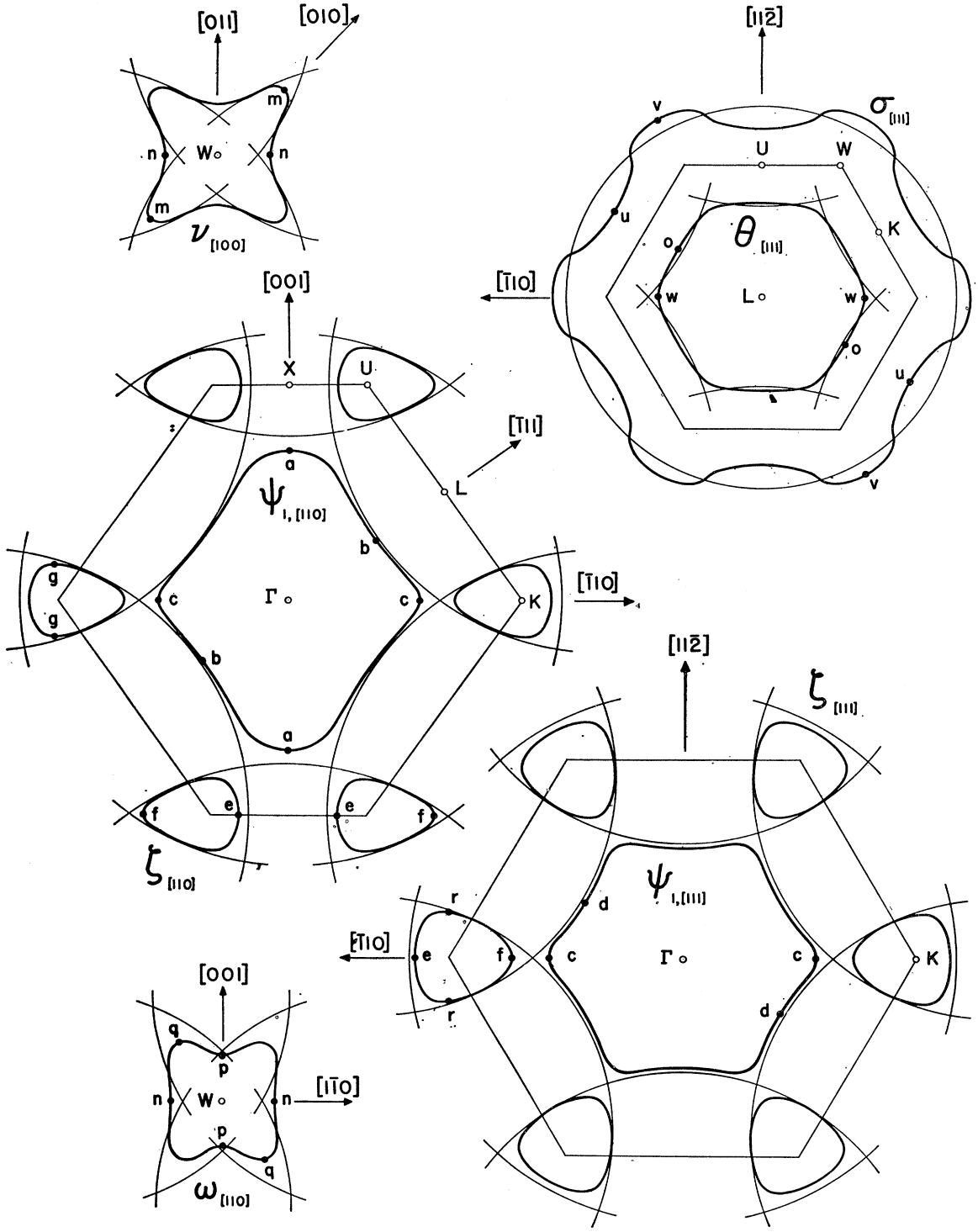

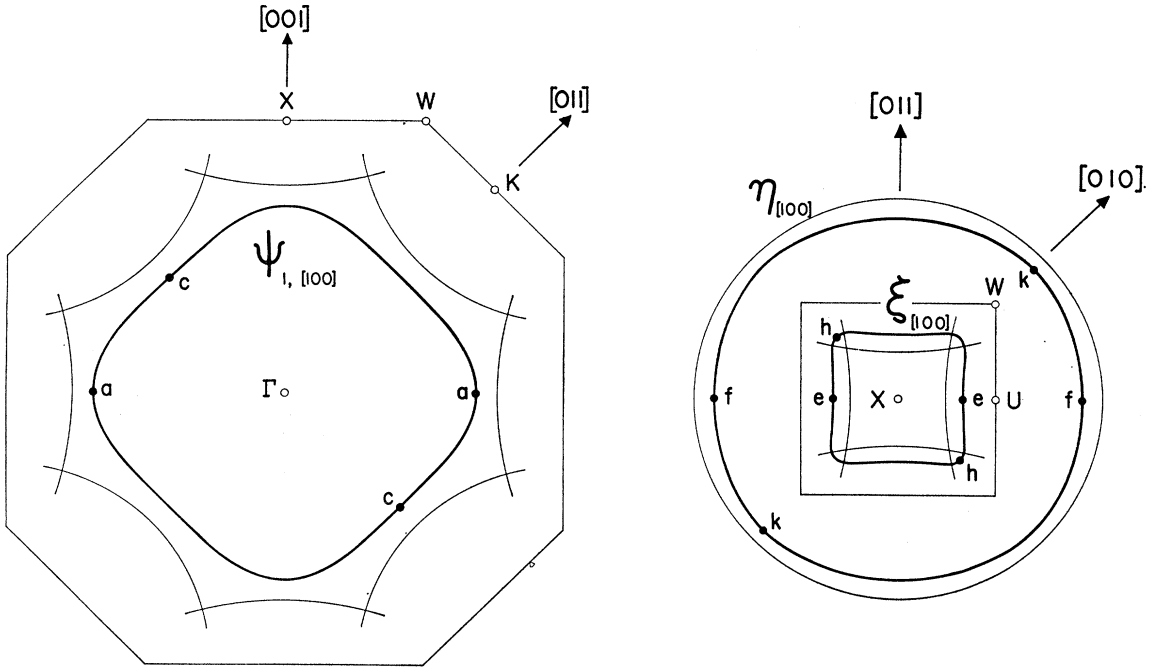

FIG. 9. The shapes of the symmetry orbits as calculated from the four-parameter model Fermi surface. The empty-lattice sections (arcs of circles) are also shown. The principal dimensions (between corresponding points labeled with small letters) are summarized in Table III.

$W_6(W_3)$ and $W_7(W_3)$, which are found to be separated by about 0.124 Ry. Also shown in Fig. 11 is the calculated Fermi level E_f, and there is a gap of about 0.015 Ry between this energy and the minimum in the fourth band $[W_7(W_2')]$; it is gratifying to find that the model can account for the apparent lack of experimental results which could be attributed to the presence of any electrons in the fourth zone.

COMPARISON WITH EXPERIMENT

(a) Detailed Shape of the Fermi Surface

The areas calculated from the four-parameter Fermi surface for the eleven possible orbits at symmetry directions are compared in Table I with those found experimentally, and in Fig. 12 we show the angular dependence of the de Haas–van Alphen periods predicted by the model Fermi surface (arrowed curves) for direct comparison with the observed period variations in the $(1\bar{1}0)$ plane. For many of the curves, the calculated and experimental periods are indistinguishable from one another within the accuracy of the experimental results. The good quantitative agreement brought about by the four-parameter model can also be appreciated by referring back to the comparison made with the empty-lattice period variations in Fig. 7; however, we note that the model Fermi surface cannot quite reproduce the very good match of the δ oscillations with the empty-lattice curve for orbit θ, but this feature is of relatively minor importance compared to the excellent over-all agreement. Also shown in Fig. 12 are the predicted limiting angles for the existence of extremal orbits; the calculated orbits cease to exist for angles which exceed by more than 0.25° the ranges shown in the figure. We have not attempted to establish precisely the limiting angles for the branch for which orbit ζ is noncentral (broken curve), since considerable

TABLE III. Principal dimensions of the Fermi surface $(2\pi/a)$.

Dimension in Fig. 9	4-parameter Fermi surface	Other experiments
aa	1.403	$1.4_4(R)$
bb	0.968	
cc	1.183	$1.4_4(R)$
dd	1.033	
ee	0.439	$0.41(R)$
ef	0.439	
ff	1.317	$1.3_0(R)$
gg	0.333	$0.37(R)$
hh	0.583	$0.31(R)$?
kk	1.547	$1.6_1(R)$
mm	0.863	
nn	0.475	
oo	0.872	
pp	0.416	
qq	0.683	
rr	0.426	
uu	1.556	
vv	1.889	$2.0_0(R)$
ww	0.940	$0.90(R)$
Γ*b* (Fig. 10)	1.248	$1.25\pm0.01(B)$, $1.25(PW)$
Γ*e* (Fig. 10)	1.190	$1.19\pm0.01(B)$, $1.18(PW)$

$(2\pi/a = 1.282\times10^8\ \text{cm}^{-1})$

R, magnetoacoustic effect (Ref. 6); *B*, Kohn effect (neutrons) (Ref. 10);
PW, Kohn effect (x rays) (Ref. 11).

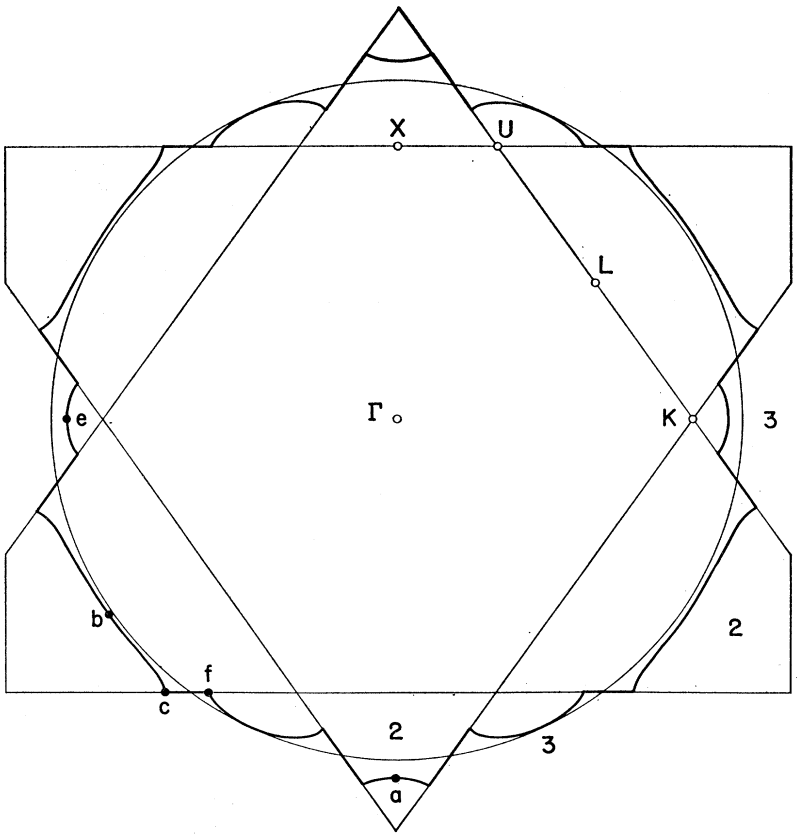

FIG. 10. The central [110] section through Γ in the extended-zone scheme. The section through the four-parameter Fermi surface (solid curves) is compared with that through the free-electron sphere (circle). The small letters correspond to those in Fig. 9.

effort would be required to find these angles reliably; a substantial effort would also have been involved in extending the curve for orbit σ to larger angles from [111].

The chief weakness of the four-parameter model is that the calculated curve for orbit ξ is found to lie significantly higher than the period values for the π oscillations; however, it was just for these oscillations that the discrepancy with the relevant empty-lattice curve was greatest (Fig. 3), and the present model certainly represents a vast improvement. Moreover, the weak π oscillations have been detected only in the immediate vicinity of [001], whereas the model predicts that the ξ orbit should exist up to a maximum of 28.5° from [001]. A further difficulty is that we have found no evidence whatsoever for any oscillations which could possibly be attributed to orbit ω; our model predicts that such period values should lie between the curves for the harmonics $\gamma^{(2)}$ and $\gamma^{(3)}$ (compare Figs. 3 and 12), but a careful search has revealed no further oscillations in this region. On the basis of rough agreement with experiment, it would seem that our tentative assignments of the weak ϵ and ϕ oscillations to orbits η and σ, respectively, are probably correct.

We have already shown in Fig. 8 that the second-zone hole surface predicted by the model has been "sandpapered" to such an extent that it will not support noncentral orbits of type ψ_2 normal to [111] (Fig. 5), and this conclusion is valid for the [001] and [110] directions as well. A similar search for noncentral orbits has also been carried out for the third-zone electron surface and the calculated variation of cross-sectional area along an arm of this surface is presented on an open scale in Fig. 13. In addition to a narrow minimum at the center of an arm (plane containing points U or K), the variation of the area becomes extremely flat at a distance of about 0.1 ($2\pi/a$) from the center before the onset of the rapid increase as one approaches a zone corner W. While the flat region is neither a maximum nor a minimum, but is rather like a region of inflection, we believe that the variation of area is nevertheless gentle enough to give rise to a de Haas–van Alphen effect. If this assumption is correct, the model would predict for the central and noncentral type-ζ orbits at [110] two periods which differ by about 2.2%. This prediction is in exact agreement with the observation of long beats with 42.5±0.5 cycles per beat in the γ oscillations at [110]. Examples of the beat patterns in the γ oscillations have been given in Ref. 1 [Figs. 1(a)–1(c)]; for an arbitrary orientation the beat envelopes are quite complex, but they reduce to a simple two-period pattern at [110]. The origin of these beats has for long been a mystery, and it is encouraging that the model Fermi surface can account for them in such a natural way.

The principal diametral dimensions of the various

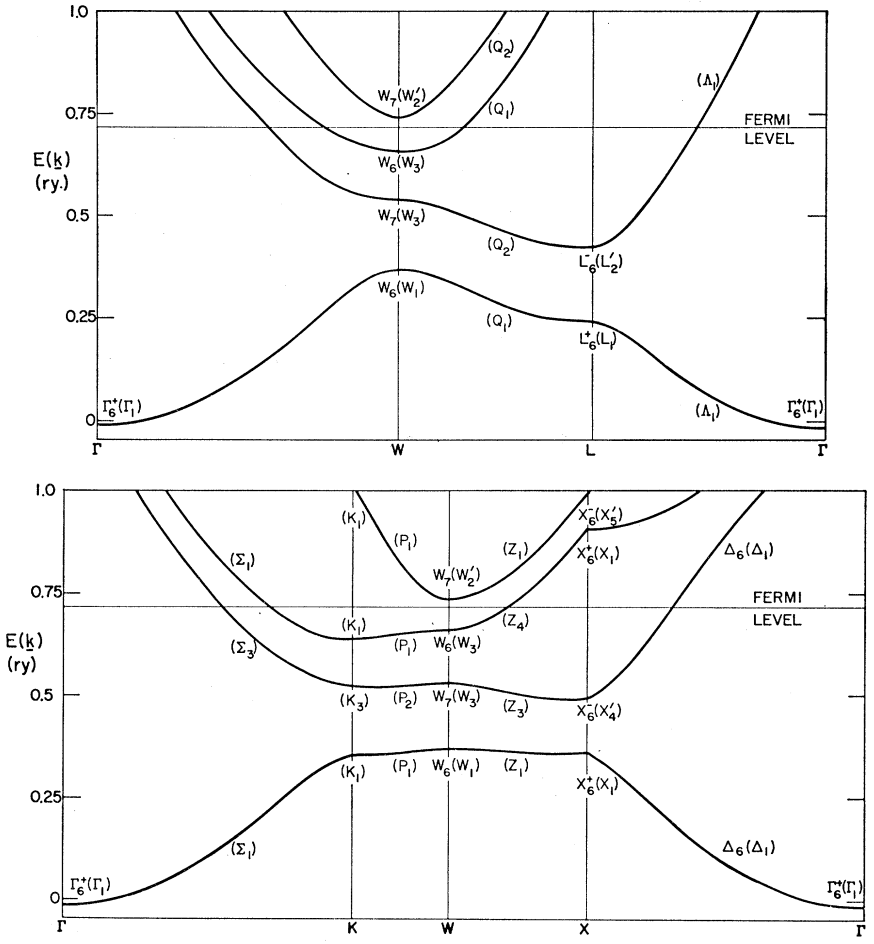

FIG. 11. Energy bands and Fermi level for lead as calculated from the four-parameter model.

symmetry sections through the model Fermi surface are summarized in Table III; the letters refer to those in Fig. 9. Where comparison can be made, the calculated dimensions are found to be in reasonable agreement with those determined directly by the magnetoacoustic effect.[5,6] Although the accuracy of the magnetoacoustic results is not very high, partly on account of the limited number of cycles which can be observed, these results usefully complement the de Haas–van Alphen measurements. In particular, it is for the large orbits η and σ that the de Haas–van Alphen results are very meager, whereas the effects of these orbits show up strongly in the magnetoacoustic effect. Although there appears to be some question of interpretation,[37] two dimensions deduced from the Kohn anomalies in the phonon spectra[9–11] are also given in Table III; these dimensions are seen to be in accord with those calculated from the model.

The arms of the multiply connected electron surface are sufficiently thick to support open orbits for certain directions of a magnetic field, and two such orbits, ρ and μ, are shown in the schematic drawing of Fig. 6. Magnetoresistance experiments[2–4] yield valuable information concerning the boundaries of the allowed field directions for the existence of these orbits, but it is rather difficult to predict these boundaries from the model Fermi surface without lengthy computer calculations. As Young has pointed out,[3] the existence of the large hole orbits of type τ (Fig. 6) at a particular orientation implies the presence of a "type-II" open orbit at that orientation. We have used the model to calculate the angular range for the occurrence of the (nonextremal) τ orbits, and find that they cease to exist beyond about 3.8° and 4.7° from [110] for field directions in the (001) and (1$\bar{1}$0) planes, respectively. On the other hand, the magnetoresistance results[4] show that the corresponding angles at the boundary of the type-II open-orbit region are considerably greater, both being about 8.15°. It is thus clear that the existence of the hole orbit τ is a sufficient but not a necessary condition for the occurrence of type-II open orbits; large extended hole orbits must play the role of orbit τ in Young's criterion in the intervening region where the τ orbits themselves no longer exist.

[37] W. A. Harrison, Phys. Rev. **129**, 2512 (1963).

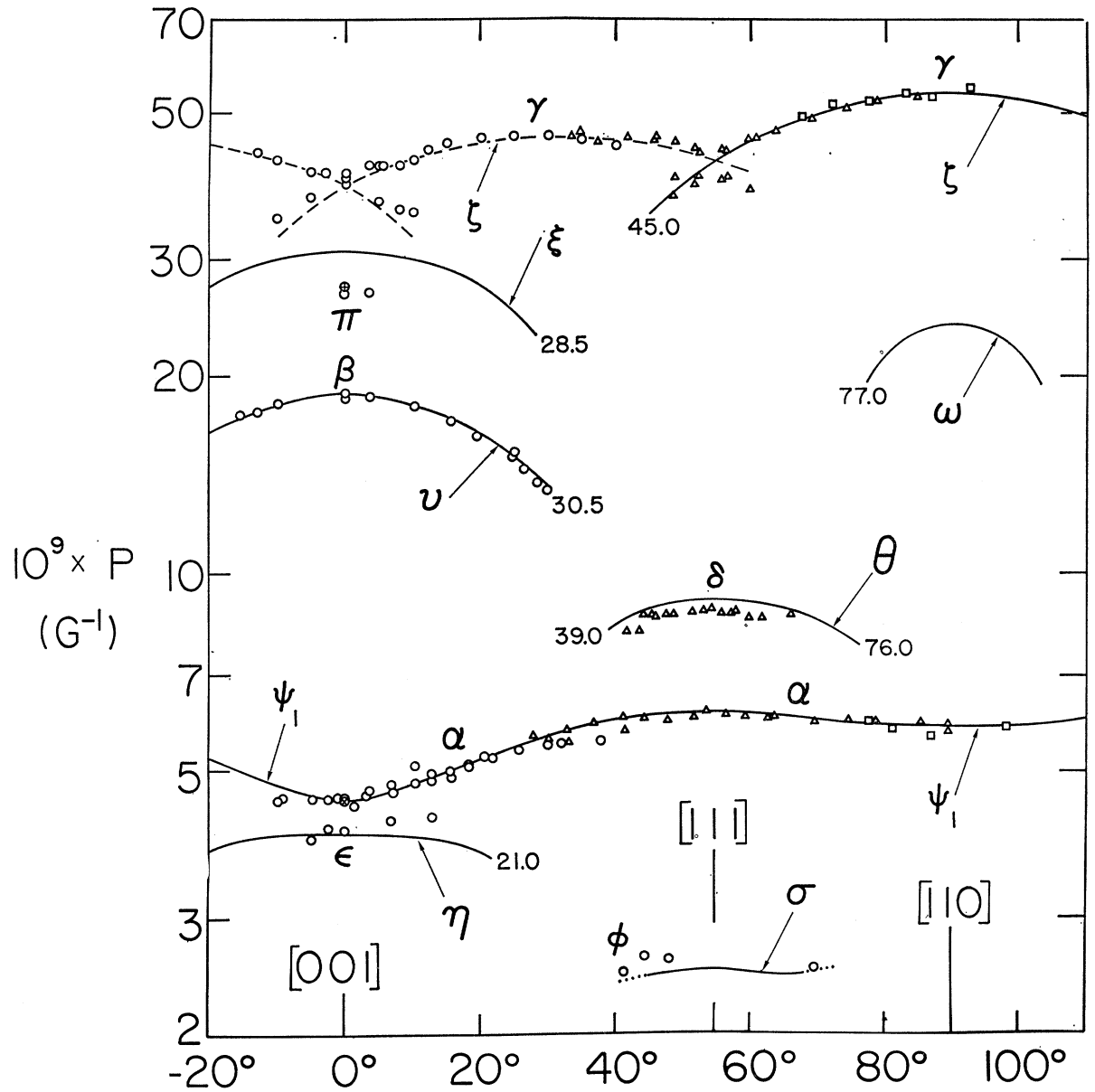

FIG. 12. A comparison of the period variations calculated from the four-parameter model (arrowed curves) with the fundamental period values from Fig. 3. The broken curves refer to orbits of type ζ which contain the symmetry points K or U but which need not be extremal with respect to area. The field directions are in the (1$\bar{1}$0) plane and the periods are plotted on a logarithmic scale; see Fig. 3 for an explanation of the symbols for the experimental points. Also shown are the limiting angles for the existence of orbits on the four-parameter Fermi surface.

(b) Differential Properties and Total Volume

Detailed studies of the orientation dependence of cyclotron resonance in lead have been carried out by Khaikin and Mina[7,8] and by Young.[3] The cyclotron mass

$$m^* = (\hbar^2/2\pi)(\partial \mathcal{A}/\partial E)_{E_f} \qquad (31)$$

measured in such experiments is evidently a differential property of the energy surfaces in the neighborhood of the Fermi level, and only those sections for which m^* is extremal contribute to the resonance. If the areas $\mathcal{A}$ of these sections are also extremal, then $\mathcal{A}_{E_f} = \mathcal{A}_0$ and direct comparison can be made between the cyclotron-resonance masses and the corresponding ones found from the temperature dependence of the de Haas–van Alphen effect[14]; with the exception of those orbits ζ whose period values follow the dashed curves in Fig. 12, symmetry requires all of the orbits which contribute to the de Haas–van Alphen effect to be extremal with respect to both $\mathcal{A}$ and m^*. We have mentioned already how information obtained from cyclotron resonance as a function of the polarization of the microwave field

TABLE IV. Cyclotron masses and curvature factors.

Oscillation orientation	Interpretation: zone, orbit	m^*/m_0 Experimental[a]	m^*/m_0 4-parameter Fermi surface	m^*/m_0 Empty-lattice model	$\frac{m^*_{\text{exp}}}{m^*_{\text{4-p.m.}}}$	$\left(\frac{\partial^2 \mathcal{A}}{\partial k_z^2}\right)_0$
α [001]	2 ψ_1	1.58(KM), 1.64(P)	0.796	0.66_8	2.02	−44.8
α [111]	2 ψ_1	1.14(KM)	0.581	0.60_2	1.96	−2.62
α [110]	2 ψ_1	1.12(KM)	0.576	0.58_6	1.94	−14.4
γ [001]	3 ζ[b]	0.74(KM), 0.75(Y) 0.68(P)	···	···	···	···
γ [111]	3 ζ	0.69(KM)	0.306	0.24_2	2.25	+1.38
γ [110]	3 ζ	0.55(KM), 0.56(Y)	0.228	0.23_3	2.41	+18.6
π [001]	3 ξ	0.90(KM), 0.85(P)	0.353	0.19_4	2.4_8	+4.48
β [001]	3 ν	1.22(KM), 1.20(P)	0.570	0.48_4	2.12	−0.29
δ [111]	3 θ	1.21(KM)	0.544	0.41_7	2.22	+4.88
ϵ [001]	3 η	2.59(KM)	1.197	1.000	2.16	−21.8
ϕ [111]	3 σ	···	1.602	1.000	···	−12.3
···[110]	3 ω	1.26(KM) or 1.41(KM) 1.35(Y)	0.591	0.52_9	2.13–2.38	+14.1
···[110]	3 κ[c]	2.47(KM)	∼1.1	···	∼2.2	···
···[110]	3 τ[c]	···	∼1.4	···	···	···

[a] KM, from cyclotron resonance (Refs. 7, 8); Y, from cyclotron resonance (Ref. 3); P, from the temperature dependence of the amplitude of the de Haas–van Alphen oscillations (R. A. Phillips, private communication).
[b] Nonextremal with respect to $\mathcal{A}$ in the empty-lattice model; for this orbit m^* could not be calculated reliably from the 4-parameter model since it was found that the position of minimum area became displaced as E_f was varied.
[c] Nonextremal with respect to $\mathcal{A}$ in both empty-lattice and 4-parameter models.

has proved helpful in confirming our interpretation of the β oscillations. In Table IV we list the cyclotron-resonance masses for the various symmetry orbits, and we also give four values of m^* found from the de Haas–van Alphen effect (detailed mass results will be published later); these four results are seen to agree well with the more reliable values obtained directly from cyclotron resonance. It is, of course, quite possible to imagine that orbits exist which may be extremal with respect to m^* but not with respect to $\mathcal{A}$; indeed Khaikin and Mina[7,8] find a resonance which they attribute to orbit κ (Fig. 6, Table IV), for which the area is certainly not stationary.

The anisotropies of those cyclotron-resonance masses which can be related to orbits of stationary area are of the same general form as the de Haas–van Alphen period variations, and they confirm in some detail the correctness of the model Fermi surface, e.g., as regards the limiting angles for the various orbits. The apparent persistence of a cyclotron resonance from orbit ν over the entire (001) plane would seem to be an exception. However the phase involved in the cyclotron resonance experiment is very low when compared to the high phase in the de Haas–van Alphen effect, and thus the former experiment does not select out such narrow groups of carriers as those which contribute in the latter. For this reason, cyclotron resonance may be observed when m^* is not exactly extremal, but only nearly so,[38] and possibly such nearly extremal orbits enable the type-ν resonance to be found near [110]. Khaikin and Mina[7,8] also report the finding of several additional resonances which do not seem to be associated with orbits of extremal area, and these resonances have not yet been satisfactorily accounted for.

From Table IV it can be seen that the masses predicted by the model band-structure do not differ much from those given by the simple empty-lattice model[14]; the only large differences occur for orbits π and σ. Also

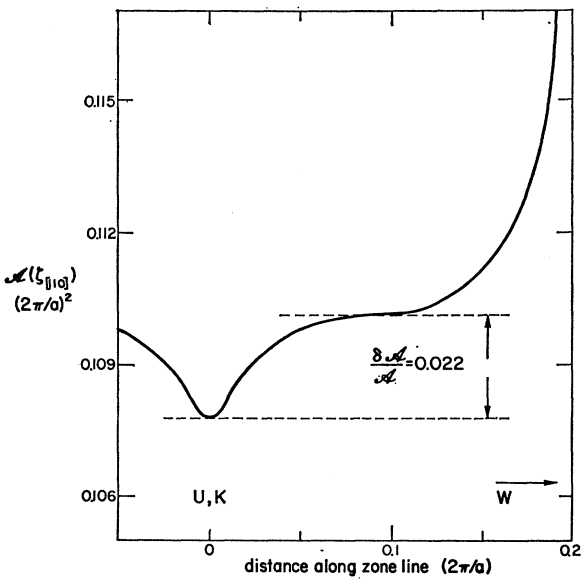

FIG. 13. Variation of the [110] area of cross section through an arm of the third-zone electron surface, as a function of the normal distance (along [110]) from the midpoint of a zone line, K or U. The curve is calculated from the model Fermi surface, with the parameter values given in Eq. (30).

[38] F. W. Spong and A. F. Kip, Phys. Rev. 137, A431 (1965).

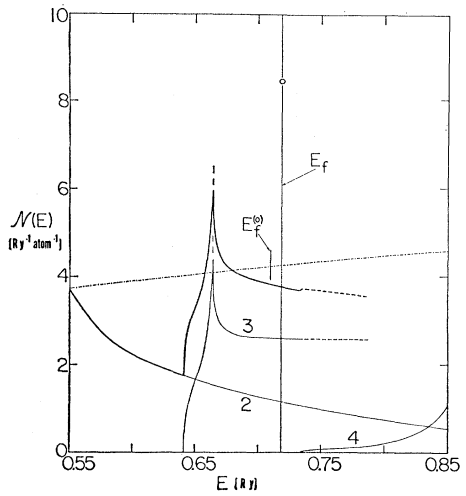

FIG. 14. The density-of-states curve in the neighborhood of the Fermi energy as calculated from the four-parameter model; the individual contributions from the second, third, and fourth bands are also shown. Dot-dash curve: free-electron model; O, from measurements of the electronic specific-heat coefficient γ (Ref. 42). The calculation of the third-band contribution is extremely awkward above the point of minimum energy in the fourth zone and it has not been carried out; however no startling changes are expected until the energy reaches $\sim$0.91 Ry (see Fig. 11). The ordinates have not been doubled to include the spin degeneracy.

given in the table are values of the ratio of the masses found experimentally to those calculated from the four-parameter model. No matter whether one considers large or small orbits on the multiply connected surface, this ratio is remarkably constant and never deviates much from 2.2; for orbits on the hole surface, the ratio appears to be about 15% smaller. The fact that the experimental and "band-structure" masses do not agree does not cause us to lose faith in the shape of the proposed Fermi surface. All along we have been regarding the mass which appears in the kinetic energy [Eq. (5)] as the free-electron mass m_0; however, if another choice were made, its sole effect would be to alter the energy scale, and hence the numerical values of the fitting parameters, but the shape of the Fermi surface would not be affected. Both the Fermi surface and the differential properties could thus be reasonably well accounted for by supposing that the mass in the kinetic energy was increased to about $2.2m_0$, at least for electrons near the Fermi surface. This type of effect is indeed expected on account of the electron-phonon interaction,[39–41] which is particularly strong for lead.

The total occupied volume in $\mathbf{k}$ space is of considerable interest, not only as a check on the consistency of the model Fermi surface but also as a prelude to determining the density-of-states curve. The volumes contained by the hole surface and by the electron surface have been calculated by integrating numerically the areas of unoccupied and occupied sections, respectively, in the smallest possible calculation region (1/48 of the Brillouin zone). The final volumes are found to correspond to 0.393 electron/atom and 0.375 hole/atom for the third and second zones, respectively. These two volumes should be identical for our model, and in fact the calculated values may be taken to be the same within the reliability of the calculation and of the four fitting parameters. The total occupied volume in the first, second and third Brillouin zones thus corresponds to $2+(2-0.375)+0.393=4.02\pm0.02$ electrons per atom. It should be remembered that E_f was not determined by conservation of electrons, but it was treated as a fitting parameter on the same footing as V_{111}, V_{200}, and λ; within the accuracy of the calculation and of the parameters, the total volume agrees, as it should, with the free-electron volume.

Values of $\mathfrak{N}(E)$, the density of electronic states, have been calculated for our model band-structure from the derivatives of the occupied volumes with respect to energy; the "Fermi energy" was treated as a variable and the other fitting parameters [Eq. (30)] were held constant. In Fig. 14 we show the contributions from the various zones to the total density-of-states curve for energies near the actual Fermi level, and as far as the general trend is concerned, the "band-structure" $\mathfrak{N}(E)$ curve does not differ much from the curve for perfectly free electrons. Also shown in the figure is the experimental value of $\mathfrak{N}(E_f)$ inferred from the electronic specific heat.[42] The experimental value is 2.23 times greater than the "band-structure" value, a discrepancy which is virtually the same as that which was found when comparing the experimental and calculated cyclotron masses (Table IV). This observation is thus in keeping with recent theoretical predictions[39–40] that the electron-phonon interaction should manifest itself in the same quantitative manner in the two phenomena. The calculated $\mathfrak{N}(E)$ curve does not show the "peaking" *at* the Fermi level which has been suggested on the basis of a crude analysis of some transport properties.[43] However, if the Fermi level were to be changed by alloying, such a peaking might indeed show up in an experimentally determined $\mathfrak{N}(E)$ curve when collisions with impurities begin to interfere seriously with the electron-phonon interaction.

CONCLUDING DISCUSSION

From the experimental information provided by the angular variations of the de Haas–van Alphen periods

[39] S. Nakajima and M. Watabe, Progr. Theoret. Phys. **30**, 772 (1963).

[40] R. E. Prange and L. P. Kadanoff, Phys. Rev. **134**, A566 (1964).

[41] J. C. Swihart, D. J. Scalapino, and Y. Wada, Phys. Rev. Letters **14**, 106 (1965).

[42] Good agreement is found between values of the electronic specific-heat coefficient γ determined calorimetrically and those determined thermodynamically from the superconducting critical-field curve. For recent determinations, which also give references to earlier work, see: N. E. Phillips, M. H. Lambert, and W. R. Gardner, Rev. Mod. Phys. **36**, 131 (1964) (calorimetry); D. L. Decker, D. E. Mapother, and R. W. Shaw, Phys. Rev. **112**, 1888 (1958) (critical fields). We have taken the value 3.05 mJ mole^{-1} deg^{-2}.

[43] A. V. Gold, Phil. Mag. **5**, 70 (1960).

in lead we have been able to arrive at a quantitative description of the Fermi surface in terms of a simple model involving only four parameters, and with this model it should be possible to make accurate calculations of any physical properties which depend directly on the geometry of the Fermi surface. Furthermore, we have seen that the model will also account reasonably well for differential properties near the Fermi energy if the free-electron mass in the kinetic energy of an electron is increased by a factor of about 2.2 to allow for the effects of the electron-phonon interaction; when this change is made, the model could be used to calculate, for example, meaningful values of the Fermi velocity at any point on the Fermi surface. The accuracies quoted for the four fitting parameters [Eq. (30)] are discussed in Appendix II, but we might point out here that the dimensions and areas of cross section predicted by the model Fermi surface will actually be more reliable than the percentage accuracies of V_{111}, V_{200}, and λ might suggest. As would be expected from the qualitative similarity with the empty-lattice model, the dimensions of the Fermi surface depend much more critically on the fourth parameter E_f, and it is this parameter which has been determined with the greatest precision.

Before any attempt is made to attach direct physical significance to the numerical values of the fitting parameters, it must be remembered that they have been evaluated within the framework of a model which is undoubtedly oversimplified. Thus any $\mathbf{k}$-dependences of the Fourier coefficients of the pseudopotential and of the spin-orbit matrix elements have been ignored (but see Appendix I for a further discussion of the spin-orbit terms), and a detailed band calculation from first principles is badly needed to check these assumptions. The spin-orbit interaction is, of course, the lowest order relativistic correction, but since it is the only correction which involves the electron spin,[44] we might expect that a fundamental relativistic calculation would yield a value for λ which is reasonably close to that given by our simple model. On the other hand, the relativistic terms of higher order are functions of coordinates only,[44] and thus their effects are implicitly incorporated in our fitted pseudopotential coefficients.

From the large spin-splitting of the levels $W_6(W_3)$ and $W_7(W_3)$, as well as from the observed trends in the numerical calculations of the areas, it is clear that in lead the spin-orbit interaction is just as effective as the ordinary lattice potential in modifying the energy bands and in creating band gaps. For our choice of normalization parameter N_2 (or N_3), the value for λ turns out to be some 50% greater than the value of the parameter ξ_{6p} for the free atom; some enhancement over ξ_{6p} might be expected because the wave function near the ion cores should be of somewhat greater amplitude in the metal since the volume of normalization is restricted to a unit cell.[45] It is also interesting to note that the value of E_f turns out to be slightly greater than the free-electron Fermi energy. A calculation by second-order perturbation theory (for $\lambda=0$) actually predicts a decrease in the Fermi energy when the effect of just one of the appropriate Bragg planes is considered.[17] However the {111} and {200} Bragg planes all intersect along lines which are very close to the Fermi surface, and thus it is perhaps unrealistic to suppose that the total change in the Fermi energy should be given by a simple superposition of the results for individual planes, Finally as far as the dependence on $|\kappa|$ is concerned. the fitted values of V_{111} and V_{200} seem to follow the trend suggested by Harrison[46] from considerations of the resistivities of various lead alloys.

In the experimental part of this study, little emphasis has been placed on obtaining information from the amplitudes of the de Haas–van Alphen oscillations. Unlike the periods, the amplitudes depend critically on the experimental conditions and their detailed behavior is not yet fully understood. Nevertheless, for the sake of completeness we have given in the last column of Table IV values of the curvature factors $\partial^2 A_0/\partial k_z^2$ predicted by the model Fermi surface; these factors and the orbit masses m^* have a large control over the final amplitudes. The very low curvature factor for orbit ν certainly helps to account for the abnormally large amplitude of the associated β oscillations, but the entries in Table IV offer no real clues as to why the π oscillations should be so weak or as to why any manifestations of orbit ω have thus far escaped observation.

ACKNOWLEDGMENTS

We have been very fortunate in enjoying the help and wise counsel of several persons throughout the duration of this study. In particular we would like to acknowledge our indebtedness to R. A. Phillips, who kindly prepared for us all of those crystals which were grown by the Czochralski technique; it was he who originally discovered the π and the $(\beta+\gamma)$ oscillations. We are also grateful to T. H. Koch for his willing assistance with the analysis of the oscillograms, and to Mrs. Marilyn Rhyne for her skilled help and advice with the programming of the various computer calculations. It was Dr. M. H. Cohen who first suggested to us several years ago that the spin-orbit effect should play an important role in lead, and it is a pleasure to thank him, Dr. W. A. Harrison, Dr. V. Heine, and Dr. J. M. Keller for helpful discussions relating to the pseudopotential, the spin-orbit interaction and group theory. Finally, one of us (J.R.A.) wishes to thank Dr. D. Shoenberg for his hospitality during a year's visit to the Royal Society Mond Laboratory, Cambridge.

[44] Cf: M. E. Rose, *Relativistic Electron Theory* (John Wiley & Sons, New York, 1961).

[45] L. Liu, Phys. Rev. **126**, 1317 (1962).

[46] W. A. Harrison, Rev. Mod. Phys. **36**, 256 (1964).

Notes added in proof.

(a) We have computed the total free area of the 4-parameter Fermi surface. In terms of the surface area of a sphere containing four electrons per atom we find that the contributions from the hole and electron surfaces are 0.220 and 0.369, respectively. The sum of these, 0.589, is in excellent agreement with Aubrey's[47] value of 0.55±0.05 from the anomalous skin effect in polycrystalline lead.

(b) A first-principles relativistic APW calculation for lead has been carried out recently by Loucks.[48] Loucks' theoretical energy bands bear strong resemblance to those predicted by the 4-parameter OPW interpolation scheme (Fig. 11), and the two sets of bands are in remarkably close agreement for energies in the neighborhood of the Fermi level.

(c) Dr. V. Heine (private communication) has suggested an alternative Hamiltonian matrix which differs from that given in Eq. (23) only by the suppression of the factors $\sqrt{2}$ in the off-diagonal spin-orbit terms [with corresponding changes in Eqs. (28)]. In our scheme, these factors are an immediate consequence of the basic requirement that the spin-orbit matrix (Eq. 20a) be Hermitian, and no further assumptions have been made regarding the normalization of the wave functions. While Heine's proposal does not appear to be consistent with our scheme, we have nevertheless investigated its merit as an alternative model for a description of the Fermi surface. The fitting parameters have been redetermined and are found to be:

$$V_{111}'=-0.085\pm0.002\text{ Ry},\quad E_f'=0.718\pm0.001\text{ Ry},$$
$$V_{200}'=-0.040\pm0.002\text{ Ry},\quad \lambda'=0.099\pm0.002\text{ Ry}.$$

Not only do these values hardly differ from those given in Eqs. (30), but also the value of $Q_{\min}$ was found to be lowered by only 10%. In fact the fit to the dominant experimental periods (areas) is just as close as in our original model; the major difference is a 3% increase in the area of the ξ orbit at [100], i.e., in the sense of improving slightly the agreement with the period of the π oscillations (Table I).

APPENDIX I: SPIN-ORBIT MATRIX ELEMENTS FOR ARBITRARY WAVE VECTOR

For any point $\mathbf{k}$, the transformation matrix which appears in Eqs. (17) and (21) is given by

$$S=\frac{1}{2}\begin{pmatrix} S_1 & S_2 \\ -S_2 & S_1^* \end{pmatrix}, \tag{AI.1}$$

where

$$S_1=\begin{bmatrix} 1 & 1 & 1 & 1 \\ 0 & 0 & i & -1 \\ 1 & 1 & -1 & -1 \\ 0 & 0 & i & -i \end{bmatrix},\quad S_2=\begin{bmatrix} 0 & 0 & 0 & 0 \\ 1 & -1 & 0 & 0 \\ 0 & 0 & 0 & 0 \\ -1 & 1 & 0 & 0 \end{bmatrix}. \tag{AI.2}$$

In order to calculate the form of the spin-orbit matrix elements for an arbitrary point $\mathbf{k}$, allowance must be made for the fact that the basis functions (16) will not in general reduce to either pure s or pure p functions in the ion-core region as they did for $\mathbf{k}=\mathbf{k}_W$. As can be readily verified by considering plane-wave expansions of the OPW's, s-p mixing appears only in the functions Φ_1' and Φ_5', and the other functions in the set (18) remain unchanged. As we leave $\mathbf{k}_W$, the two affected functions are given by

$$\Phi_1',\Phi_5' \rightarrow [N_s\psi_s+N_p\{(k_x-\tfrac{1}{2})\psi_{p_x}+k_y\psi_{p_y}+(k_z-1)\psi_{p_z}\}]\alpha_1,\alpha_2. \tag{AI.3}$$

In our problem the relative strength N_p/N_s of the p-like and s-like contributions is not known *a priori*, and if $N_p\neq0$ the functions (AI.3) may not be orthogonal to the other wave functions in the set. The matrix elements are readily evaluated as before, and in the spin-orbit part of the Hamiltonian (20) we now have

$$\mathcal{H}_{so}'=\begin{pmatrix} A_{so} & B_{so} \\ -B_{so} & A_{so}^* \end{pmatrix}, \tag{AI.4}$$

where

$$A_{so}=\lambda/2\begin{bmatrix} 0 & -iN_pN_{2\frac{1}{2}}(\beta+\beta^*) & iN_pN_{3\frac{1}{2}}(\beta+\beta^*) & -2N_pN_2(k_x-\pi/a)+iN_pN_{2\frac{1}{2}}(\beta+\beta^*) \\ iN_pN_{2\frac{1}{2}}(\beta+\beta^*) & 2N_2^2 & 0 & 0 \\ -iN_pN_{3\frac{1}{2}}(\beta+\beta^*) & 0 & 0 & -2N_2/N_3 \\ -2N_pN_3(k_x-\pi/a)-iN_pN_{2\frac{1}{2}}(\beta+\beta^*) & 0 & -N_3/N_2 & -2N_2^2 \end{bmatrix} \tag{AI.5}$$

and

$$B_{so}=\lambda/2\begin{bmatrix} 0 & -iN_pN_{2\frac{1}{2}}(\beta-\beta^*) & iN_pN_{3\frac{1}{2}}(\beta-\beta^*) & iN_pN_{2\frac{1}{2}}(\beta-\beta^*) \\ iN_pN_{2\frac{1}{2}}(\beta-\beta^*) & 0 & 0 & 0 \\ -iN_pN_{3\frac{1}{2}}(\beta-\beta^*) & 0 & 0 & 0 \\ -iN_pN_{2\frac{1}{2}}(\beta-\beta^*) & 0 & 0 & 0 \end{bmatrix}. \tag{AI.6}$$

[47] J. E. Aubrey, Phil. Mag. 8, 1001 (1960).
[48] T. L. Loucks, Phys. Rev. Letters 14, 1072 (1965).

Here $\beta=k_y-i(k_z-(2\pi/a))$. We note that $B_{so}=0$ on the plane $k_z=2\pi/a$ and N_s enters the calculations only through the normalization of the wave functions. We have set $N_2=\sqrt{2}/2$ and $N_3=1$ as explained in the text.

For our model Fermi surface we have simply taken $N_p=0$, and in order to make some check on the validity of this simplifying assumption, we have calculated the areas of the eleven symmetry orbits taking $N_p=0.5$ and using the same values of the parameters which were obtained from the best fit for $N_p=0$ [Eq. (30)]. The results for $N_p=0.5$ are given in brackets in Table I, and it can be seen that these area values are almost identical to those for $N_p=0$, i.e., the shape of the Fermi surface is evidently not very sensitive to the choice of this parameter. Strictly speaking, the parameter values should all be redetermined for each choice of N_p, but the very tedious computations which would be involved do not seem justified in view of the close agreement between the two sets of calculated areas in Table I.

A somewhat simpler approach for estimating the spin-orbit matrix elements was tried initially, in which it was assumed that in the core region the OPW's could be represented by functions of the form

$$N\mathbf{p}\cdot\mathbf{k}\alpha_i, \tag{AI.7}$$

where N is a normalization coefficient and $\mathbf{p}\cdot\mathbf{k}$ is the projection of an atomic p function in the direction $\mathbf{k}$. In this approach the wave functions in the core region have the same symmetry as the OPW's, but any s contribution to the wave function is neglected. However, with the choice (AI.7) for arbitrary $\mathbf{k}$, the results did not match up properly with those calculated for the point W using the basis set (18) and this simplified approach had to be abandoned.

APPENDIX II: THE LEAST-SQUARES ITERATION CALCULATION AND ACCURACY OF THE FITTING PARAMETERS

The sum of the weighted squared deviations Q [Eq. (29)] for the eight principal symmetry orbits was minimized subject to the simplifying assumption that in the neighborhood of $Q_{\min}$ each of the calculated areas was a linear function of the fitting parameters. When all the calculated and experimental areas $\mathcal{A}^i$ are normalized by dividing by the corresponding experimental uncertainties $\delta\mathcal{A}^i$ (Table I), we may write

$$\alpha_{\text{calc}}{}^i(X_j+\delta X_j)=\alpha_{\text{calc}}{}^i(X_j)+B_{ij}\delta X_j, \tag{AII.1}$$

where X_j stands for a trial set of the parameters λ, E_f, V_{111}, and V_{200}, and $B_{ij}=\partial\alpha_{\text{calc}}{}^i/\partial X_j$. The least-squares solution for the changes δX_j which would be required to bring Q to $Q_{\min}$ is, in matrix form,[49]

$$\boldsymbol{\delta X}=-(\tilde{B}B)^{-1}\tilde{B}\mathbf{C}=W\mathbf{C}, \tag{AII.2}$$

where the element in the ith row of the column vector $\mathbf{C}$ is $\alpha_{\text{calc}}{}^i(X)-\alpha_{\text{exp}}{}^i$.

The initial trial values of the parameters X_j were the coordinates of the point at which an approximate minimum in Q had been found by rough graphical interpolations (see main text). However, while some of the calculated areas were found to vary linearly with some parameters, others did not, and for this reason $Q_{\min}$ had to be approached by an iterative process. For each iteration, the X_j were changed by one-twentieth of the predicted δX_j, and the areas $\mathcal{A}_{\text{calc}}{}^i$ and the derivatives B_{ij} were re-evaluated at each stage. The variance-covariance matrix $W\tilde{W}=(\tilde{B}B)^{-1}$ was also evaluated after each iteration, and the process was repeated until the square of any predicted change δX_j became typically less than 10% of the smallest element in the row (or column) of $W\tilde{W}$ appropriate to that variable X_j.

When the iteration calculation was terminated, the matrix $W\tilde{W}$ had the numerical value given below, in units of 10^{-6} Ry^2,

X	λ	E_f	V_{111}	V_{200}
λ	3.96	1.02	−2.46	−0.54
E_f	1.02	0.72	−0.32	−0.89
V_{111}	−2.46	−0.32	3.29	−1.74
V_{200}	−0.54	−0.89	−1.74	2.93

(AII.3)

There is evidently a strong covariance between the parameters since all the elements are more or less of the same magnitude. Had there been no covariance, $W\tilde{W}$ would have been diagonal, and the standard deviations of the parameter values would have been given by the square roots of the appropriate diagonal elements; however, in order to give some indication of the uncertainties involved, we have simply quoted in Eq. (30) the square roots of the diagonal elements of the nondiagonal matrix (AII.3). It must be remembered that the least-squares fit was made to only eight symmetry orbits, whereas if *all* the period values in the $(1\bar{1}0)$ plane had been taken into account, the almost perfect fit for the α, β, and γ oscillations (Fig. 12) would have resulted in much smaller uncertainties in the parameters. On the other hand, the agreement with the δ period values is not quite so good, and the discrepancy between the π period values and those calculated for orbit ξ should not be overlooked. For these and similar reasons, we believe that the uncertainties quoted in Eq. (30) are quite realistic. No doubt slightly different parameter values would have been found if the total occupied volume had been constrained to correspond to exactly four electrons per atom throughout the least-squares fitting procedure; the volume constraint was not incorporated because of the prohibitive amount of computer time which would have been involved in arriving at accurate volume values for each step in the iterative fitting calculation.

[49] Cf: O. Kempthorne, *Design and Analysis of Experiments* (John Wiley & Sons, New York, 1952), Chap. 5.

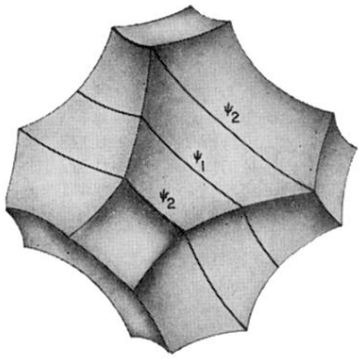

FIG. 5. The empty-lattice hole surface in the second zone (to scale). ψ_1, central [111] extremal orbit; ψ_2, noncentral [111] extremal orbit.

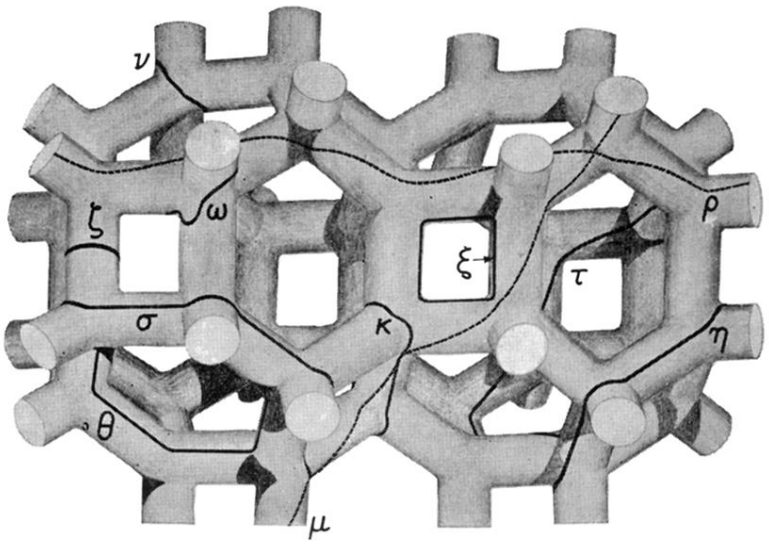

FIG. 6. A portion of the empty-lattice electron surface in the third zone (schematic). The orbits κ and τ are nonextremal with respect to area, and the broken curves depict the open orbits ρ and μ.